indicates a heat capacity change at −30.6 °C (T'_g) in the first scan. The second scan of the frozen solution shifted the transition to a slightly higher temperature (1–3 °C), suggesting further concentration of the solutes upon heat treatment. The frozen solutions containing rHA only or higher concentrations of rHA did not exhibit apparent T'_g transitions in the scans both before and after the heat treatment, as reported in other protein solutions [16,30]. The gradual endothermic shift of the thermogram from approximately −23 °C suggests continuous physical property changes (e.g., melting of surrounding ice) of the freeze-concentrated protein solutions. Analysis using other methods often produces T'_g values of frozen protein solutions ranging from −12 to −8 °C [30]. These frozen solutions also showed smaller thermal transitions at −50 to −40 °C (data not shown). While the origin of the thermal event is under active discussions, the broad nature of these lower temperature transitions prevented detailed analysis in this study [31].

Most of the trehalose-rich and equivalent concentrations of rHA and trehalose mixture frozen solutions exhibited single T'_g transitions that suggested mixing of the freeze-concentrated solutes at varied temperatures during the first scans. However, a frozen trehalose-dominant solution (i.e., 20 mg/mL rHA, 180 mg/mL trehalose) showed two peaks at the T'_g temperature range found in the first scan. Heat treatment of some trehalose-rich frozen solutions (e.g., 40 mg/mL rHA, 160 mg/mL trehalose) at −5 °C (30 min) induced two transition peaks in the subsequent heating scans. The relative magnitude of the higher temperature transition, as indicated by the area under the peak of the first derivative curve, increased with increasing rHA concentration ratio. Annealing only slightly (up to 2 °C) shifted the single transition in other frozen solutions. The single and double peaks should indicate T'_g transitions of the miscible and phase-separated concentrated phases that differ in the solute compositions. Broad single peaks in the boundary concentration ratio solutions (e.g., 80 mg/mL rHA, 120 mg/mL trehalose) suggest the overlapping of the multiple transitions upon heat treatment. Changing the buffer from 5 mM histidine-HCl to 10 mM sodium phosphate (pH 7.0) did not apparently alter the thermal properties of the heat-treated rHA and trehalose mixture frozen solutions (data not shown).

The effects of the heat treatment temperature and time on the thermal properties of the frozen rHA (40 mg/mL) and trehalose (160 mg/mL) mixture solutions were studied. Fig. 2 shows the derivative thermograms obtained in the scans prior to and after the heat treatment at −5 °C for 1–480 min. The frozen solutions retained the single T'_g after the shorter heat treatments, whereas longer exposure to the elevated temperature resulted in two transitions at approximately −28 and −25 °C in the subsequent heating scan. Further holding at −5 °C resulted in the broadening of the two transition peaks. Heat treatment at −25 to −5 °C resulted in apparent changes in the thermal properties at higher temperatures (−10 °C<, 30 min) (Fig. 3). Some frozen solutions exhibited slower phase separation when annealed at the lower temperature (−15 °C, 120, and 480 min, data not shown). The apparent effect of the heat treatment temperature and time indicates the contribution of the increasing solute mobility at temperatures far above T'_g to the solute miscibility change. The 100 mg/mL rHA and trehalose mixture frozen solution retained the single T'_g peak even with long heat treatment times (e.g., −5 °C, 480 min), indicating practical stability of the freeze-concentrated mixture (data not shown).

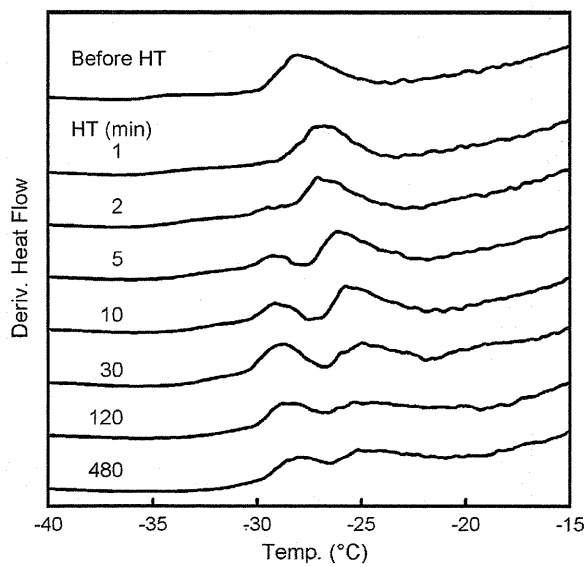

Fig. 2. Derivative thermograms of frozen solutions containing 40 mg/mL rHA and 160 mg/mL trehalose (5 mM histidine-HCl buffer, pH 7.0, 10 μL) obtained in the heating scans (5 °C/min) prior to and after heat treatment at −5 °C for 1–480 min.

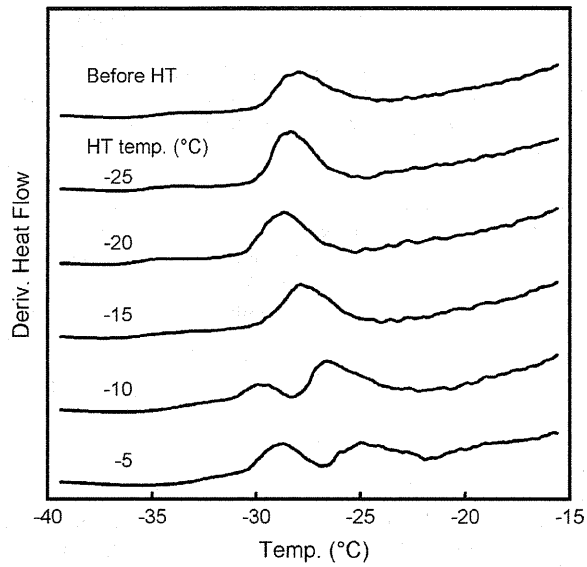

Fig. 3. Derivative thermograms of frozen solutions containing 40 mg/mL rHA and 160 mg/mL trehalose (5 mM histidine-HCl buffer, pH 7.0, 10 μL) obtained in the heating scans (5 °C/min) prior to and after heat treatment at −25 °C to −5 °C for 30 min.

Various protein and disaccharide mixture frozen solutions were subjected to thermal analysis at different weight concentration ratios to examine the effects of heat treatment (Fig. 4). Some frozen solutions showed single or no apparent transitions. The profiles of the transition temperatures obtained in the heating scans prior to and after the heat treatment (−5 °C, 30 min) revealed similar physical property changes of the systems that depend largely on the concentration ratio. Heat-treated trehalose-rich rHA and trehalose mixture solutions (total 100 and 200 mg/mL) exhibited their lower temperature transitions (T'_{g2L}) close to that of single-solute frozen trehalose solution (approximately −30 °C), which should indicate the transition of the phase dominant in trehalose. The higher temperature event (T'_{g2H}) always appeared at around −25 °C, indicating that a phase of constant composition formed post-annealing irrespective of the initial solution composition. In addition, the plots of T'_g vs. the disaccharide mass fraction suggest that the extent of the phase separation is minimal when the mass fractions are 0.5 or lower. The threshold of the T'_g profiles suggests that the solute mixture phase retains up to 1:1 disaccharide/protein weight concentration ratios of rHA and trehalose upon heat treatment. The relative contribution of the solute compositions to the

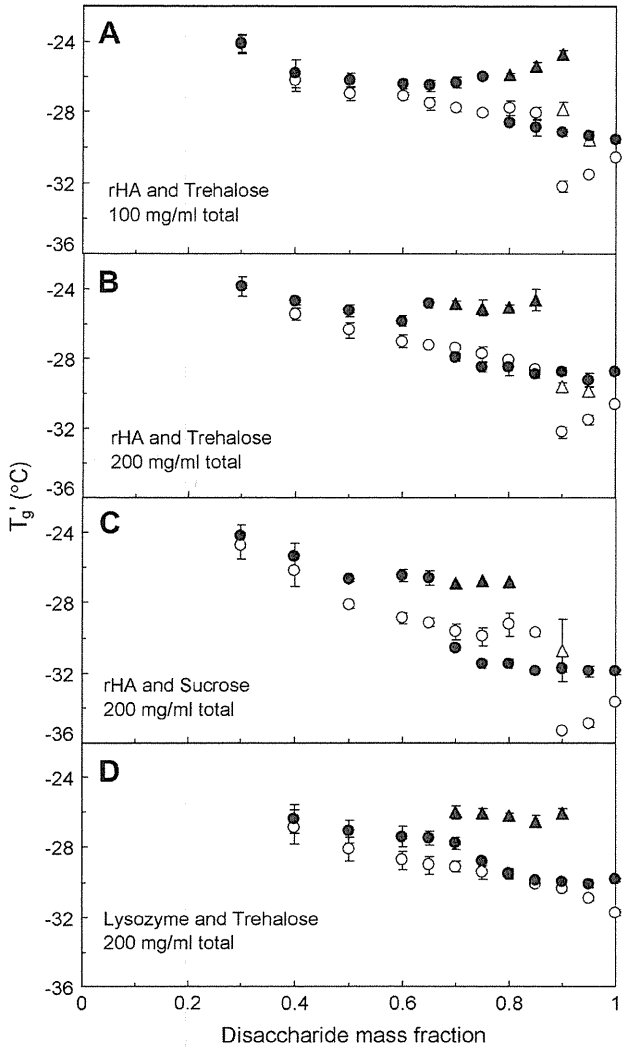

Fig. 4. Transition temperature profiles of frozen protein (rHA, lysozyme) and disaccharide (trehalose, sucrose) mixture frozen solutions (10 μL) obtained in the heating scans (5 °C/min) prior to (T'_{g1L}: ○, T'_{g1H}: △) and after (T'_{g2L}: ●, T'_{g2H}: ▲) heat treatment at −5 °C for 30 min. The total concentration of protein and disaccharide was 100 or 200 mg/mL (n = 3, average ± s.d.).

annealing-induced changes in miscibility was compared at two different compositions (total concentrations of 100 and 200 mg/mL). Other disaccharide-rich mixture frozen solutions of protein and disaccharides (e.g., rHA and sucrose, lysozyme and trehalose) also exhibited the two T'_g upon heat treatment. The lower intrinsic transition temperature of sucrose relative to that of trehalose should also lower the T'_g of the two phases. The transition temperature profiles were similar to those of dextran and disaccharides observed in a previous study [25].

The effect of NaCl, which is often included in lyophilized formulations for protein solubilization or to provide physiological osmolarity, on the thermal properties of rHA and trehalose mixtures was studied. Fig. 5 shows the derivative thermograms of frozen solutions containing 40 mg/mL rHA, 160 mg/mL trehalose, and 0–250 mM NaCl obtained prior to and after heat treatment at −5 °C for 30 min. The salt lowered the single transition temperature obtained in the first heating scans, presumably because of the plasticizing effect [32]. Higher concentrations of salt lowered and broadened the two T'_g transitions of the heat-treated frozen solutions, suggesting the distribution of the salt to the miscible and phase-separated freeze-concentrated phases.

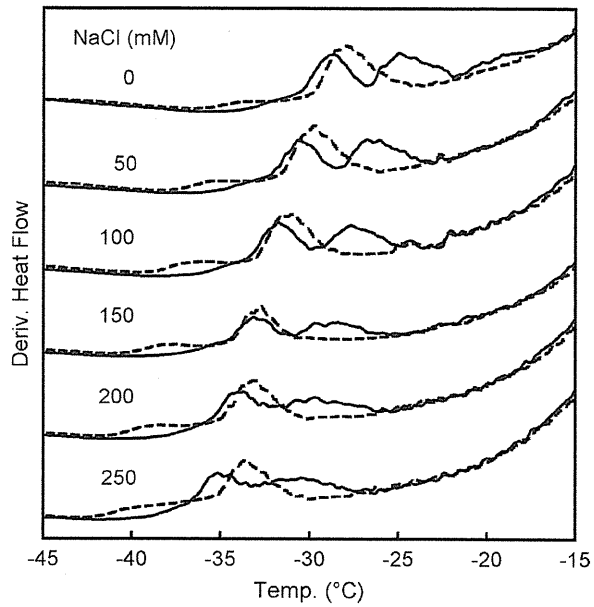

Fig. 5. Effect of various concentrations of NaCl (0–250 mM) on the derivative thermograms of frozen solutions containing 40 mg/mL recombinant human albumin and 160 mg/mL trehalose obtained in the heating scans (5 °C/min) prior to (dotted lines) and after (solid lines) heat treatment at −5 °C for 30 min.

3.2. Effects of heat treatment on immunoglobulin and disaccharide miscibility

The effects of post-freezing heat treatment were also studied in the solutions containing an immunoglobulin (i.e., bovine plasma IgG and recombinant humanized IgG1k monoclonal antibody) and trehalose in the presence of NaCl and the pH buffer salt. The disaccharide-rich mixture frozen solutions (20–60 mg/mL bIgG, 140–180 mg/mL trehalose) exhibited the two T'_g transitions upon

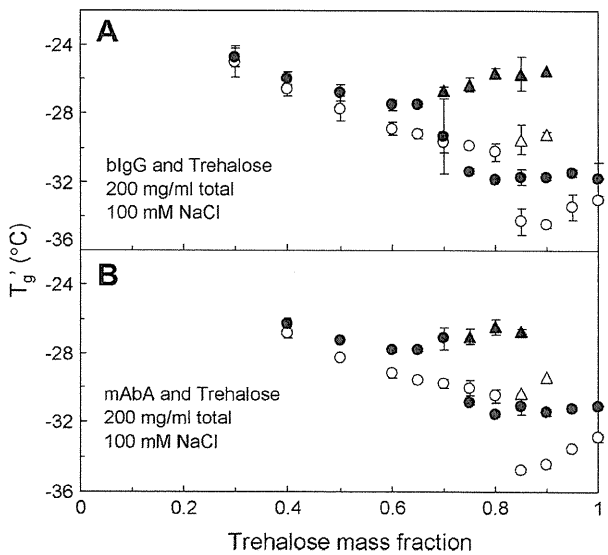

Fig. 6. Transition temperature profiles of frozen solutions containing an immunoglobulin (bIgG, mAbA), trehalose, NaCl (100 mM), and histidine-HCl buffer (5 mM, pH 7.0, 10 μL) obtained in the heating scans (5 °C/min) prior to (T'_{g1L}: ○, T'_{g1H}: △) and after (T'_{g2L}: ●, T'_{g2H}: ▲) heat treatment at −5 °C for 30 min. The total concentration of immunoglobulin and trehalose was 200 mg/mL (n = 3, average ± s.d.).

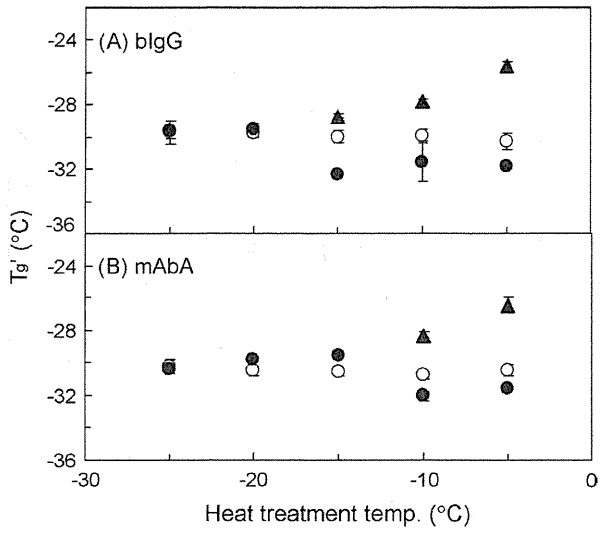

Fig. 7. Effect of heat treatment temperature on the T'_g of frozen solutions containing an immunoglobulin (bIgG, mAbA, 40 mg/mL), trehalose (160 mg/mL), 100 mM NaCl, and 5 mM histidine-HCl buffer (pH 7.0) obtained in the heating scans (5 °C/min) prior to (T'_{g1}: ○) and after (T'_{g2L}: ●, T'_{g2H}: ▲) heat treatment at −25 to −5 °C for 30 min ($n = 3$, average ± s.d.).

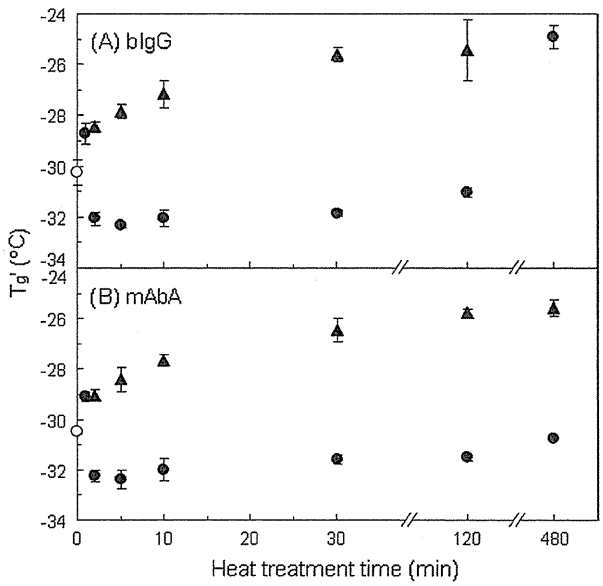

Fig. 8. Effect of heat treatment time on the T'_g of frozen solutions containing an immunoglobulin (bIgG, mAbA, 40 mg/mL), trehalose (160 mg/mL), 100 mM NaCl, and 5 mM histidine-HCl buffer (pH 7.0) obtained in the heating scans (5 °C/min) prior to (T'_{g1}: ○) and after (T'_{g2L}: ●, T'_{g2H}: ▲) heat treatment at −5 °C ($n = 3$, average ± s.d.).

heat treatment at −5 °C for 30 min (Fig. 6). In contrast, the heat treatment only slightly shifted the transition of frozen solutions containing equivalent concentrations of bIgG and trehalose to higher temperatures. No thermal transitions indicative of either the crystallization or melting of NaCl dihydrate-ice were observed over the concentration range employed in the experiments.

Figs. 7 and 8 show the effects of heat treatment temperature and time on the transition temperatures of the frozen immunoglobulin and trehalose mixture solutions (e.g., 40 mg/mL bIgG or mAbA, 160 mg/mL trehalose, 100 mM NaCl, 5 mM L-histidine buffer). The frozen solution showed the two T'_g transitions upon longer and higher temperature heat treatment as observed in the albumin systems. The systems containing trehalose and the two immunoglobulins exhibited similar propensity for the annealing-induced solute phase separation. The lower temperature transition (T'_{g2L}) became broad and unclear with longer heat treatments (>120 min) of the frozen solutions (data not shown). The gradual changes of thermograms observed after longer heat treatments suggest continuous changes in the phase composition in NaCl-containing systems.

4. Discussion

The post-freeze heat treatment induced phase separation of some protein and disaccharide mixture systems relevant for pharmaceutical formulations. The higher transition temperature phase should contain the protein and disaccharide molecules [25]. When the composition of protein–disaccharide solutions exceeds a certain ratio, phase separation leads to the formation of disaccharide-rich and protein-rich phases, which correspond to lower and higher T'_g events observed during heating post-annealing. Clarifying the mechanism of the phenomena and its effect on the formulation quality should assist rational design and manufacturing of lyophilized pharmaceuticals.

4.1. Possible mechanism of the annealing-induced solute phase separation

Freezing many multi-solute aqueous solutions, which often starts from −5 to −25 °C, concentrates the solutes into highly viscous supercooled solutions surrounding ice crystals in relatively short time periods. Our studies indicated two mechanisms that induce multiple non-crystalline concentrated solute phases in a frozen solution. The increasing concentrations during the ice growth separate some polymer systems (e.g., PVP and dextran) into multiple supercooled phases rich in one of the component polymers, resulting in two T'_g transition peaks in the following heating scans [14,33]. Cooling other systems, including those containing disaccharides and proteins, should kinetically trap the solutes in a highly viscous miscible phase, which exhibits a single T'_g. On annealing of disaccharide-rich compositions above their T'_g, an increase in the mobility within the freeze concentrate should facilitate a separation into thermodynamically favorable disaccharide-rich and protein-rich phases. In addition, a decrease in the viscosity could enable limited ice crystallization (i.e., devitrification) during annealing. On the contrary, annealing should keep some protein-rich and equivalent concentration ratio mixtures in the single concentrated phase.

The cause of the two transitions obtained in the first scans of some disaccharide-dominant mixture frozen solutions (10–30 mg/mL rHA, 170–190 mg/mL disaccharide) remains unclear. Our preliminary experiments suggest that the solution volume and cooling speed also influence the thermal behavior of the solutions during warming (data not shown). The relationship between the thermal analysis conditions and physical properties of frozen solutions remains to be elucidated.

4.2. Factors determining protein and disaccharide miscibility

The solute miscibility in the freeze-concentrates may depend on the magnitude and nature of protein-excipient, protein–protein, and excipient–excipient interactions in the hydrated environment (e.g., hydrogen bonding, hydrophobic interactions, and van der Waals interactions). Factors that influence these interactions include protein and excipient structure, solute concentration in the

unfrozen fraction, and other solution conditions such as temperature, ionic strength, pH, and the type of salt [14,16,34,35]. When excipient–excipient interactions are more favorable than protein–excipient interactions, phase separation may occur. The proteins and disaccharides are suggested to be mixed up to approximately 1:1 disaccharide/protein weight concentration ratio after heat treatment (Figs. 4 and 6). This ratio is consistent with the reported maximum ratio of disaccharides interacting directly with the protein molecules in the freeze-dried solids obtained experimentally through spectroscopic methods, water–vapor sorption measurement, and molecular modeling approaches based on the number of hydrogen bonds [36–38].

4.3. Implications in pharmaceutical lyophilization

The annealing-induced post-freezing phase separation should affect the stability of proteins during the formulation process and subsequent storage in various ways. Many freeze-dried antibody formulations contain 1:1 or 1:2 mass ratio of protein and disaccharide. The results suggest that the ingredients in these formulations separate into multiple phases or remain miscible upon annealing of the frozen solutions depending largely on the composition. Possible difference in the thermal history of the small thermal analysis solutions and solutions in formulation vials should affect the occurrence of the phase separation. The disaccharide molecules in the solute mixture phase should maintain the hetero-molecular hydrogen bonding that substitute water molecules. It, however, remains unclear whether the excipients provide sufficient interaction to protect the protein conformation throughout the process and during storage [39–42]. Possible changes in the local environment, including the co-solute compositions (e.g., inorganic salts and pH modifiers) and their mobility in the mixture phase, should alter the protein stability. Lower transition temperatures of the disaccharide phase in the frozen solutions and dried solids can adversely affect physical and chemical stability of the system during the process and subsequent storage. Freeze-drying of the phase-separated frozen solutions should also require appropriate process control to ensure the efficient ice sublimation and physical integrity of the resulting solids [43–45].

5. Conclusion

In this study, we found that sucrose and trehalose, which are the most commonly used excipients in lyophilized therapeutic protein formulations, and proteins can undergo post-freeze annealing-induced phase separation. The increasing mobility of solutes and melting of surrounding ice during heat treatment should allow spatial reordering of the freeze-concentrated proteins and disaccharides toward more thermodynamically stable states. The results clearly indicate that the application of post-freeze annealing requires sufficient understanding of its effects on the quality of products, including protein stability during processing and storage. In conclusion, the phase separation of protein and disaccharide combinations in frozen solutions should be considered an important factor when developing freeze-dried formulations.

Acknowledgement

This work was supported in part by the Japan Health Sciences Foundation.

References

[1] M.J. Pikal, Mechanism of protein stabilization during freeze-drying and storage: the relative importance of thermodynamic stabilization and glassy state relaxation dynamics, in: L. Rey, J.C. May (Eds.), Freeze-drying/Lyophilization of Pharmaceutical and Biological Products, Marcel Dekker, New York, 1999, pp. 161–198.
[2] J.F. Carpenter, K. Izutsu, T.W. Randolph, Freezing- and drying-induced perturbations of protein structure and mechanisms of protein protection by stabilizing additives, in: L. Rey, J.C. May (Eds.), Freeze-drying/Lyophilization of Pharmaceutical and Biological Products, Marcel Dekker, New York, 1999, pp. 123–160.
[3] B.S. Chang, R.M. Beauvais, A. Dong, J.F. Carpenter, Physical factors affecting the storage stability of freeze-dried interleukin-1 receptor antagonist: glass transition and protein conformation, Arch. Biochem. Biophys. 331 (1996) 249–258.
[4] J.F. Carpenter, J.H. Crowe, An infrared spectroscopic study of the interactions of carbohydrates with dried proteins, Biochemistry 28 (1989) 3916–3922.
[5] S.N. Timasheff, Stabilization of protein structure by solvent additives, in: T. Ahern, M.C. Manning (Eds.), Stability of Protein Pharmaceuticals, Plenum, New York, 1992, pp. 265–285.
[6] T. Arakawa, S.J. Prestrelski, W.C. Kenney, J.F. Carpenter, Factors affecting short-term and long-term stabilities of proteins, Adv. Drug Deliv. Rev. 46 (2001) 307–326.
[7] S. Ohtake, Y. Kita, T. Arakawa, Interactions of formulation excipients with proteins in solution and in the dried state, Adv. Drug Deliv. Rev. 63 (2011) 1053–1073.
[8] A.P. MacKenzie, Non-equilibrium freezing behaviour of aqueous systems, Philos. Trans. R. Soc. Lond. B 278 (1971) 167–189.
[9] H. Levine, L. Slade, Thermomechanical properties of small-carbohydrate–water glasses and 'rubbers', J. Chem. Soc. Faraday Trans. 1 (84) (1988) 2619–2633.
[10] L.M. Her, M. Deras, S.L. Nail, Electrolyte-induced changes in glass transition temperatures of freeze-concentrated solutes, Pharm. Res. 12 (1995) 768–772.
[11] M.C. Heller, J.F. Carpenter, T.W. Randolph, Effects of phase separating systems on lyophilized hemoglobin, J. Pharm. Sci. 85 (1996) 1358–1362.
[12] K. Izutsu, S. Yoshioka, S. Kojima, T.W. Randolph, J.F. Carpenter, Effects of sugars and polymers on crystallization of poly(ethylene glycol) in frozen solutions: phase separation between incompatible polymers, Pharm. Res. 13 (1996) 1393–1400.
[13] T.W. Randolph, Phase separation of excipients during lyophilization: effects on protein stability, J. Pharm. Sci. 86 (1997) 1198–1203.
[14] K. Izutsu, M. Heller, T.W. Randolph, J.F. Carpenter, Effect of salts and sugars on phase separation of polyvinylpyrrolidone-dextran solutions induced by freeze-concentration, J. Chem. Soc. Faraday Trans. 94 (1998) 411–418.
[15] M.C. Heller, J.F. Carpenter, T.W. Randolph, Application of a thermodynamic model to the prediction of phase separations in freeze-concentrated formulations for protein lyophilization, Arch. Biochem. Biophys. 363 (1999) 191–201.
[16] K. Izutsu, S. Kojima, Freeze-concentration separates proteins and polymer excipients into different amorphous phases, Pharm. Res. 17 (2000) 1316–1322.
[17] K. Izutsu, C. Yomota, T. Kawanishi, Impact of heat treatment on the physical properties of noncrystalline multisolute systems concentrated in frozen aqueous solutions, J. Pharm. Sci. 100 (2011) 5244–5253.
[18] N. Perez-Moral, C. Adnet, T.R. Noel, R. Parker, The aggregative stability of β-lactoglobulin in glassy mixtures with sucrose, trehalose and dextran, Eur. J. Pharm. Biopharm. 78 (2011) 264–270.
[19] B.S. Bhatnagar, S.W. Martin, T.S. Hodge, T.K. Das, L. Joseph, D.L. Teagarden, E.Y. Shalaev, R. Suryanarayanan, Investigation of PEG crystallization in frozen and freeze-dried PEGylated recombinant human growth hormone-sucrose systems: implications on storage stability, J. Pharm. Sci. 100 (2011) 3062–3075.
[20] S.L. Shamblin, L.S. Taylor, G. Zografi, Mixing behavior of colyophilized binary systems, J. Pharm. Sci. 87 (1998) 694–701.
[21] A.M. Padilla, I. Ivanisevic, Y. Yang, D. Engers, R.H. Bogner, M.J. Pikal, The study of phase separation in amorphous freeze-dried systems. Part I: Raman mapping and computational analysis of XRPD data in model polymer systems, J. Pharm. Sci. 100 (2011) 206–222.
[22] L.S. Taylor, G. Zografi, Sugar–polymer hydrogen bond interactions in lyophilized amorphous mixtures, J. Pharm. Sci. 87 (1998) 1615–1621.
[23] N. Jovanović, A. Gerich, A. Bouchard, W. Jiskoot, Near-infrared imaging for studying homogeneity of protein–sugar mixtures, Pharm. Res. 23 (2006) 2002–2013.
[24] D.S. Katayama, J.F. Carpenter, K.P. Menard, M.C. Manning, T.W. Randolph, Mixing properties of lyophilized protein systems: a spectroscopic and calorimetric study, J. Pharm. Sci. 98 (2009) 2954–2969.
[25] K. Izutsu, C. Yomota, T. Kawanishi, Impact of heat treatment on the physical properties of noncrystalline multisolute systems concentrated in frozen aqueous solutions, J. Pharm. Sci. 100 (2011) 5244–5253.
[26] A.M. Padilla, M.J. Pikal, The study of phase separation in amorphous freeze-dried systems, Part 2: Investigation of Raman mapping as a tool for studying amorphous phase separation in freeze-dried protein formulations, J. Pharm. Sci. 100 (2011) 1467–1474.
[27] V. Ragoonanan, A. Aksan, Heterogeneity in desiccated solutions: implications for biostabilization, Biophys. J. 94 (2008) 2212–2227.
[28] J. Dong, A. Hubel, J.C. Bischof, A. Aksan, Freezing-induced phase separation and spatial microheterogeneity in protein solutions, J. Phys. Chem. B 113 (2009) 10081–10087.
[29] M.J. Akers, V. Vasudevan, M. Stickelmeyer, Formulation development of protein dosage forms, Pharm. Biotechnol. 14 (2002) 47–127.
[30] B.S. Chang, C.S. Randall, Use of subambient thermal analysis to optimize protein lyophilization, Cryobiology 29 (1992) 632–656.

[31] A. Pyne, R. Suryanarayanan, The effect of additives on the crystallization of cefazolin sodium during freeze-drying, Pharm. Res. 20 (2003) 283–291.
[32] S.L. Nail, S. Jiang, S. Chongprasert, S.A. Knopp, Fundamentals of freeze-drying, Pharm. Biotechnol. 14 (2002) 281–360.
[33] K. Izutsu, N. Aoyagi, S. Kojima, Effect of polymer size and cosolutes on phase separation of poly(vinylpyrrolidone) (PVP) and dextran in frozen solutions, J. Pharm. Sci. 94 (2005) 709–717.
[34] B.Y. Zaslavsky, Aqueous Two-phase Partitioning, Marcel Dekker, New York, 1995.
[35] V. Tolstoguzov, Compositions and phase diagrams for aqueous systems based on proteins and polysaccharides, Int. Rev. Cytol. 192 (2000) 3–31.
[36] B. Wang, S. Tchessalov, N.W. Warne, M.J. Pikal, Impact of sucrose level on storage stability of proteins in freeze-dried solids: I. Correlation of protein–sugar interaction with native structure preservation, J. Pharm. Sci. 98 (2009) 3131–3144.
[37] K.R. Ward, G.D. Adams, H.O. Alpar, W.J. Irwin, Protection of the enzyme L-asparaginase during lyophilisation – a molecular modelling approach to predict required level of lyoprotectant, Int. J. Pharm. 187 (1999) 153–162.
[38] L.L. Chang, D. Shepherd, J. Sun, D. Ouellette, K.L. Grant, X.C. Tang, M.J. Pikal, Mechanism of protein stabilization by sugars during freeze-drying and storage: native structure preservation, specific interaction, and/or immobilization in a glassy matrix?, J Pharm. Sci. 94 (2005) 1427–1444.
[39] B.S. Chang, G. Reeder, J.F. Carpenter, Development of a stable freeze-dried formulation of recombinant human interleukin-1 receptor antagonist, Pharm. Res. 13 (1996) 243–249.
[40] J.L. Cleland, X. Lam, B. Kendrick, J. Yang, T.H. Yang, D. Overcashier, D. Brooks, C. Hsu, J.F. Carpenter, A specific molar ratio of stabilizer to protein is required for storage stability of a lyophilized monoclonal antibody, J. Pharm. Sci. 90 (2001) 310–321.
[41] S.U. Sane, R. Wong, C.C. Hsu, Raman spectroscopic characterization of drying-induced structural changes in a therapeutic antibody: correlating structural changes with long-term stability, J. Pharm. Sci. 93 (2004) 1005–1018.
[42] J.D. Andya, C.C. Hsu, S.J. Shire, Mechanisms of aggregate formation and carbohydrate excipient stabilization of lyophilized humanized monoclonal antibody formulations, AAPS PharmSci 5 (2003) E10.
[43] K. Schersch, O. Betz, P. Garidel, S. Muehlau, S. Bassarab, G. Winter, Systematic investigation of the effect of lyophilizate collapse on pharmaceutically relevant proteins I: stability after freeze-drying, J. Pharm. Sci. 99 (2010) 2256–2278.
[44] E. Meister, H. Gieseler, Freeze-dry microscopy of protein/sugar mixtures: drying behavior, interpretation of collapse temperatures and a comparison to corresponding glass transition data, J. Pharm. Sci. 98 (2009) 3072–3087.
[45] K. Izutsu, K. Fujii, C. Katori, C. Yomota, T. Kawanishi, Y. Yoshihashi, E. Yonemochi, K. Terada, Effects of solute miscibility on the micro- and macroscopic structural integrity of freeze-dried solids, J. Pharm. Sci. 99 (2010) 4710–4719.

Biochimica et Biophysica Acta 1840 (2014) 1171–1180

Contents lists available at ScienceDirect

Biochimica et Biophysica Acta

journal homepage: www.elsevier.com/locate/bbagen

Physicochemical properties and in vitro intestinal permeability properties and intestinal cell toxicity of silica particles, performed in simulated gastrointestinal fluids

Kumiko Sakai-Kato [a,*], Masayuki Hidaka [a], Keita Un [a], Toru Kawanishi [b], Haruhiro Okuda [b]

[a] Division of Drugs, National Institute of Health Sciences, 1-18-1 Kamiyoga, Setagaya-ku, Tokyo 158-8501, Japan
[b] National Institute of Health Sciences, 1-18-1 Kamiyoga, Setagaya-ku, Tokyo 158-8501, Japan

ARTICLE INFO

Article history:
Received 11 July 2013
Received in revised form 10 December 2013
Accepted 13 December 2013
Available online 19 December 2013

Keywords:
Nanomaterial
Silica particle
In vitro model
Simulated gastrointestinal fluid

ABSTRACT

Background: Amorphous silica particles with the primary dimensions of a few tens of nm, have been widely applied as additives in various fields including medicine and food. Especially, they have been widely applied in powders for making tablets and to coat tablets. However, their behavior and biological effects in the gastrointestinal tracts associated with oral administration remains unknown.
Methods: Amorphous silica particles with diameters of 50, 100, and 200 nm were incubated in the fasted-state and fed-state simulated gastric and intestinal fluids. The sizes, intracellular transport into Caco-2 cells (model cells for intestinal absorption), the Caco-2 monolayer membrane permeability, and the cytotoxicity against Caco-2 cells were then evaluated for the silica particles.
Results: Silica particles agglomerated in fed-state simultaneous intestinal fluids. The agglomeration and increased particles size inhibited the particles' absorption into the Caco-2 cells or particles' transport through the Caco-2 cells. The in vitro cytotoxicity of silica particles was not observed when the average size was larger than 100 nm, independent of the fluid and the concentration.
Conclusion: Our study indicated the effect of diet on the agglomeration of silica particles. The sizes of silica particles affected the particles' absorption into or transport through the Caco-2 cells, and cytotoxicity in vitro, depending on the various biological fluids.
General significance: The findings obtained from our study may offer valuable information to evaluate the behavior of silica particles in the gastrointestinal tracts or safety of medicines or foods containing these materials as additives.

1. Introduction

Nanomaterials are materials that have at least one dimension in the nanoscale range (approximately 1 nm to 100 nm). Recently, nanomaterials have been applied in various fields, including medicine, cosmetics, and foods, because nanomaterials may have physical, chemical, or biological properties that are different from those of their bulk. While nanotechnology can exploit the improved and often novel properties of materials, there have been publications about concerns regarding the safety to humans and potential environmental impact of such materials [1–4].

In the medical field, nanomaterials have been used as drug carriers for drug delivery systems (DDS) [5–8].

Amorphous silica particles have been widely applied as additives for various purposes, for example, to improve the flowability used in powders for making tablets; they have also been applied as additives to coat tablets, to improve their hardness. In solid oral dosage form, silicates are often used as glidants. Glidants are substances that improve the flowability of cohesive powders and granules. Silicates are well suited for that purpose, because of their small particle size and large specific surface area. One of the most frequently used glidants is colloidal silica (e.g., Aerosil 200), which exhibits very small particle sizes in the nanometer range, and a large specific surface area of approximately 200 m^2/g [9]. Although the primary dimensions of these particles are a few tens of nm, they form aggregates of a few hundred nm. These novel materials have been the focus of medical developments in a number of areas, and many researchers have investigated their use not only as additives in tablets, but also as novel carriers for poorly-water-soluble drugs [10–12].

Amorphous silica particles have also been used in other fields, where they are applied directly to the human body as ingredients in cosmetics and toothpaste, or even as powdered food ingredients to prevent caking [13,14].

Abbreviations: DDS, drug delivery system; PDI, polydispersity index; TEM, transmission electron microscopy; FaSSGF, fasted-state simulated gastric fluids; FeSSGF, fed-state simulated gastric fluids; FaSSIF, fasted-state simulated intestinal fluids; FeSSIF, fed-state simulated intestinal fluids; DMEM, Dulbecco's modified Eagle's medium; PBS, Phosphate buffer saline; HBSS, Hanks' balanced salt solution; FBS, fetal bovine serum; TEER, transepithelial electrical resistance

* Corresponding author. Tel./fax: +81 3 3700 9662.
E-mail address: kumikato@nihs.go.jp (K. Sakai-Kato).

0304-4165/$ – see front matter © 2013 Elsevier B.V. All rights reserved.
http://dx.doi.org/10.1016/j.bbagen.2013.12.014

However, when amorphous silica particles were swabbed on skin, it was reported that the nano-sized materials penetrated through the skin, became distributed in the body, and induced unexpected toxicity [2]. It has been reported that the toxicity derived from amorphous silica particles depends on the particle size and the surface properties [15,16].

Generally, tablets are taken via oral administration. Using this administration route, the particles contained in the tablets do not remain at specific sites for a long period. However, if the particles are absorbed from the intestine and enter the blood circulation, it is important to consider whether the phenomena that occur when the drugs are administered intravenously would also occur in this case. In addition, no studies have been performed to investigate the toxicity associated with the oral administration of amorphous silica particles as additives in oral solid dosage forms; the evaluation of the physicochemical properties, intestinal permeability properties, and intestinal cell toxicity resulting from the oral administration of nano- or submicron-size amorphous silica particles is therefore essential to ensure the safety of solid oral dosage forms containing these materials.

In the present study, we evaluated the size, the absorption from the intestine, and the cytotoxicity using in vitro models of amorphous silica particles after oral administration. In particular, we investigated the effects of the size of the particles and the composition of the intestinal tract fluid on the intestinal permeability properties and the intestinal cell toxicity. In this study, we used amorphous silica particles with diameters of 50, 100, and 200 nm. In the oral administration of medicines, the physiological conditions in the intestinal tract are dramatically different in the fasted state and the fed state. It is known that these differences affect the absorption of drugs from the gastrointestinal tract. This study therefore investigated the changes in the size of amorphous silica particles in the fasted-state and fed-state simulated gastric and intestinal fluids.

As an in vitro model for intestinal absorption, we used the Caco-2 cell. Caco-2 cells grown as a monolayer become differentiated and polarized such that their morphological and functional phenotype resembles that of the enterocytes that line the small intestine [17,18]. Caco-2 cells express tight junctions, microvilli, and numerous enzymes and transporters that are characteristic of such enterocytes. The Caco-2 monolayer is widely used throughout the pharmaceutical industry as an in vitro model of the human small intestinal mucosa to predict the absorption of orally administered drugs. The correlation between the in vitro apparent permeability across Caco-2 monolayers and the in vivo fraction absorbed is well established [19]. Caco-2 cells have in fact been used as a model to investigate the possible harmful effect of silica nanoparticles in the gastrointestinal tract [20]. Furthermore, Caco-2 monolayers have been used to evaluate the intracellular uptake of nanosized-drug delivery systems [21,22].

In this study, the intracellular transport into Caco-2 cells, the Caco-2 monolayer membrane permeability, and the cytotoxicity against Caco-2 cells were then evaluated for the amorphous silica particles, in the fasted-state and fed-state simulated gastric and intestinal fluids.

2. Materials and methods

2.1. Silica particles

Suspensions of fluorescently labeled amorphous silica particles (nominal diameters as stated by suppliers: 50 nm, SP-50; 100 nm, SP-100; and 200 nm, SP-200) were obtained from Micromod Partikeltechnologie (Rostock, Germany). These were amorphous silica particles [16]. Silica suspensions were shaded and stored at 4 °C and diluted in various fluids before each experiment. The suspensions were sonicated for 10 min, and then vortexed for 1 min immediately prior to use. The silica particles were suspended in various fluids, and then incubated at 37 °C for 1 h before the measurements were performed. The mean particle size, the polydiversity index (PDI), and the ζ-potentials of the silica particles were measured using a Zetasizer Nano-ZS (Malvern Instruments, UK), with a concentration of 0.1 mg/mL in water (Table 1). The water used in this study was purified using Milli-Q system (Millipore, Tokyo, Japan). Fig. 1 shows transmission electron microscopy (TEM) images of the silica particles used in this study. The images were obtained using an H-9000 UHR instrument (Hitachi, Tokyo, Japan).

Table 1
The mean particle size, the polydiversity index (PDI), and the ζ-potentials of the silica particles used in this study.

Sample	Particle size (nm)	PDI	ζ-Potential
Silica			
SP-50	47.5 ± 4.0	0.14 ± 0.053	−43.2 ± 2.0
SP-100	99.0 ± 3.2	0.03 ± 0.030	−53.8 ± 1.4
SP-200	176 ± 6.4	0.16 ± 0.024	−51.8 ± 1.4

Samples were dissolved in MilliQ water with a concentration of 0.1 mg/mL.
Each value represents the mean ± S.D. ($n = 3$).

2.2. Cell culture

Caco-2 cells—human epithelial colorectal adenocarcinoma cells (American Type Culture Collection (ATCC), Manassas, VA, USA)—were cultured in Dulbecco's modified Eagle's medium (Life Technologies, Brooklyn, NY, USA) supplemented with 10% FBS (Nichirei Biosciences, Tokyo, Japan), 100 U/ml penicillin/streptomycin (Life Technologies). Cells were grown in a humidified incubator at 37 °C under 5% CO_2, and the culture medium was changed every other day.

2.3. Composition of simulated gastric and intestinal fluids

The fasted-state simulated gastric fluids (FaSSGF) and the fed-state simulated gastric fluids (FeSSGF) were prepared according to a previous report [23]. The fasted-state simulated intestinal fluids (FaSSIF) and the fed-state simulated intestinal fluids (FeSSIF) were prepared according to the manufacturer's instructions (Celeste Co., Tokyo, Japan). An Ubbelohde-type viscometer was used for the viscosity measurements. The detailed components of each fluid are shown in Table 2.

2.4. Stability of fluorescence labeling

Fluorescently labeled silica particles were diluted to 1 mg/mL in various types of fluids (MilliQ water, D-MEM, PBS, FaSSIF, FeSSIF, FaSSGF, FeSSGF, 0.25% trypsin-ethylenediamine tetraacetic acid, and lysis buffer (1.0% Triton X-100 in HBSS)) and incubated at 37 °C for 6 h. After incubation, the particles were centrifuged (20,000 g, 30 min) and the precipitated silica particles were resuspended with the same volumes of fresh fluids as those before centrifugation. The fluorescent intensities of the suspension before and after centrifugation were measured at an excitation wavelength of 542 nm and an emission wavelength of 602 nm in a fluorescence spectrophotometer (F-7000; Hitachi High-Technologies, Tokyo, Japan). The percentage of the fluorescent dye retained in the silica particles after 6-h incubation was expressed as follows:

$$A/B \times 100(\%),$$

where A represents the fluorescence intensity of the silica particles resuspended with fresh fluid after centrifugation, and B represents the fluorescence intensity of the silica suspension before centrifugation.

2.5. Intracellular uptake study

Fluorescently labeled silica particles were used in this study to evaluate the intracellular uptake of silica particles. Caco-2 cells (1×10^6) were plated in a 6-well plate in medium containing 10% FBS and 100 U/mL penicillin/streptomycin. The fluorescently labeled silica particles were diluted to a concentration of 0.1 mg/mL in various types of fluids (D-MEM, PBS, FaSSIF, and FeSSIF), and then incubated at 37 °C for 1 h to mimic the intestinal conditions. In addition, to mimic the

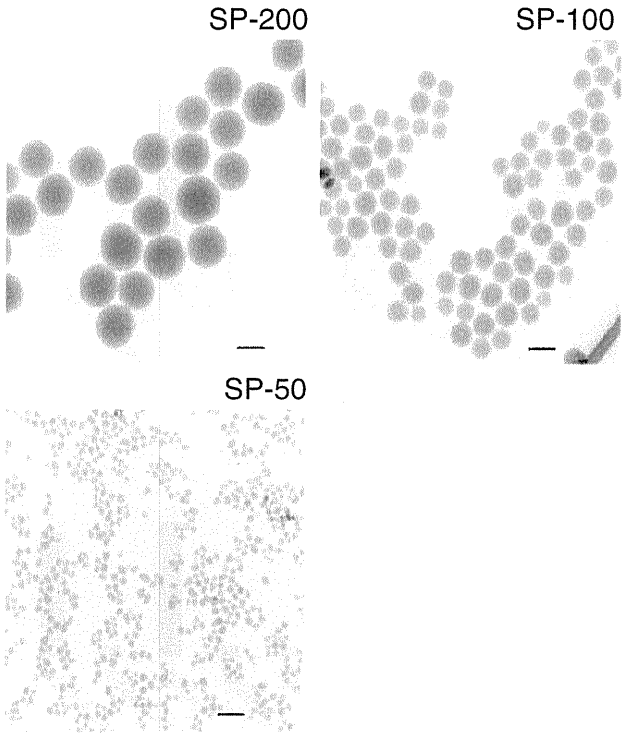

Fig. 1. TEM images of silica particles used in this study. The scale bar represents 100 nm.

gastric and intestinal conditions (indicated as "FaSSGF → FaSSIF" and "FeSSGF → FeSSIF"), fluorescently labeled silica particles were diluted to 10 mg/mL in FaSSGF or FeSSGF, and incubated at 37 °C for 1 h. Subsequently, the diluted silica particles were further diluted to a concentration of 0.1 mg/mL in FaSSIF or FeSSIF, and incubated at 37 °C for an additional 1 h. The diluted and incubated fluorescently labeled silica particles were added to the cells, which were pre-incubated for 96 h (37 °C, 5% CO_2). After incubation for 2 h in the silica particle-containing fluid, the cells were washed, and the incubation medium was replaced with Hanks' balanced salt solution (HBSS). The cells were then trypsinized with 0.25% trypsin-ethylenediamine tetraacetic acid (Life Technologies), washed with HBSS three times, and suspended in lysis buffer (1.0% Triton X-100 in HBSS). The cell suspension was shaken, centrifuged at 15,000 ×*g* and 4 °C for 10 min, and the fluorescence intensity of the resulting supernatant was measured at an excitation wavelength of 542 nm and an emission wavelength of 602 nm in a fluorescence spectrophotometer (F-7000). The fluorescence intensity was expressed as incorporated particle mass per unit protein content of cells. The protein concentration was determined using a protein assay kit (Dojindo Molecular Technologies, Tokyo, Japan).

Table 2
Composition of FaSSGF, FeSSGF, FaSSIF, and FeSSIF.

	FaSSGE	FeSSGF	FaSSIF	FeSSIF
Sodium taurocholate (μM)	80	–	3	15
Sodium acetate (mM)	–	29.75	–	–
Sodium chloride (mM)	34.2	237.02	105.4	203.1
Sodium hydroxide (mM)	–		10.5	101
Sodium dihydrogen-orthophosphate (mM)			28.7	
Acetic acid (mM)		17.12	–	144.17
Lecithin (μM)	20	–	0.75	3.75
Pepsin (mg/mL)	0.1	–	–	–
pH	1.6	5	6.5	5.0
Osmolality (mOsm/kg)	120.7 ± 2.5	400	270 ± 10	635 ± 10

2.6. Confocal microscopy study

To observe the intracellular uptake of the fluorescently labeled silica particles, Caco-2 cells (5.0×10^4) were plated in 35 mm glass-bottom dishes coated with poly-L-lysine (Matsunami Glass, Osaka, Japan) in medium containing 10% FBS and 100 U/mL penicillin/streptomycin. The fluorescently labeled silica particles were diluted to a concentration of 0.1 mg/mL in various types of fluids (PBS, FaSSIF, and FeSSIF), and then incubated at 37 °C for 1 h to mimic the intestinal conditions. After the cells were pre-incubated for 48 h (37 °C, 5% CO_2), the diluted and incubated fluorescently labeled silica particles were added to the cells. After incubation for 2 h in the silica particle-containing fluid (37 °C or 4 °C, 5% CO_2), the cells were washed and kept in HBSS for imaging using confocal microscopy (Carl Zeiss LSM 510, Oberkochen, Germany). To observe co-localization, endosomes and lysosomes of cells were labeled with AlexaFluor-488-conjugated transferrin (Life Technologies) and LysoTracker Green DND-26 (Life Technologies), respectively, in accordance with the manufacturer's instructions. Data were collected using dedicated software supplied by the manufacturers, and exported in tagged image file format.

2.7. Transcellular transport study

Caco-2 cells were suspended in a serum-free medium consisting of D-MEM and Mito + Serum Extender (BD Biosciences, San Jose, CA, USA), and seeded on 24-well size BD Falcon cell culture inserts (BD Biosciences) at 2×10^5 cells/well [24]. In experiments that required the use of differentiation medium, the seeding medium was replaced with optimized differentiation medium 48 h after cell seeding; the medium was replaced every 24 h thereafter. The transepithelial electrical resistance (TEER) was also measured using a Millicell-ERS resistance system (Millipore, Billerica, MA, USA) every 24 h, and the wells with TEER values of over 200 Ω cm^2 were used as Caco-2 cell monolayers. The fluorescently labeled silica particles were diluted to a concentration of 1 mg/mL in various types of fluids (PBS, FaSSIF, and FeSSIF), and then incubated at 37 °C for 1 h to mimic the intestinal conditions. In addition, to mimic the gastric and intestinal conditions (indicated as "FaSSGF → FaSSIF" and "FeSSGF → FeSSIF"), fluorescently labeled silica particles were diluted to 10 mg/mL in FaSSGF or FeSSGF, and incubated at 37 °C for 1 h. The diluted silica particles were subsequently further diluted to a concentration of 1 mg/mL in FaSSIF or FeSSIF, and incubated at 37 °C for an additional 1 h. The diluted and incubated fluorescently labeled silica particles were added to the apical side of the Caco-2 cell monolayers. Phosphate buffer saline (PBS) was added to the basal side at the same time. Samples (fluorescently labeled silica particles) were drawn out of the basal side at 15 min intervals. An equal volume of PBS was added to the basal side immediately after each sampling. The TEER was simultaneously determined using a Millicell-ERS resistance system.

2.8. Cytotoxicity study

The cytotoxicity of the silica particles was assessed using a WST-8 assay (Cell Counting Kit-8, Dojindo Laboratories, Kumamoto, Japan). Caco-2 cells (1×10^5) were plated in 96-well plate in medium containing 10% FBS and 100 U/mL penicillin/streptomycin. Silica particles were diluted to concentrations of 0.1, 1, or 10 mg/mL in various types of fluids (D-MEM, PBS, FaSSIF, and FeSSIF), and incubated at 37 °C for 1 h to mimic the intestinal conditions. In addition, to mimic the gastric and intestinal conditions (indicated as "FaSSGF → FaSSIF" and "FeSSGF → FeSSIF"), silica particles were diluted to 10 mg/mL in FaSSGF or FeSSGF, and incubated at 37 °C for 1 h. The diluted silica particles were subsequently further diluted to concentrations of 0.1 or 1 mg/mL in FaSSIF or FeSSIF, and incubated at 37 °C for an additional 1 h. After the cells were pre-incubated for 72 h (37 °C, 5% CO_2), the diluted and subsequently incubated particles were added to the cells. After

incubation for 6 h, the cells were washed, the fluid was replaced with fresh culture medium without silica particles, and an additional 0, 6, 24, or 48 h of incubation was applied. Cell counting kit-8 solutions were then added to each well, and the cells were incubated for 2 h. After incubation, absorbance values at 450 nm were measured using a microplate reader (Bio-Rad Laboratories, Hercules, CA, USA), and the results were expressed as viability (%).

2.9. Statistical analyses

The results are presented here as the mean ± S.D., calculated from more than three experiments. An analysis of variance (ANOVA) was used to test the statistical significance of the differences between groups. Multiple comparisons between control and test groups were performed using Dunnett's test.

3. Results

3.1. Effects of simulated gastric and intestinal fluids on the size of silica particles

The effects of various fluids on the size of the amorphous silica particles were evaluated. Following the dispersion of the silica particle samples (nominal diameters: 50 nm, SP-50; 100 nm, SP-100; and 200 nm, SP-200, as stated by the supplier) SP-50, SP-100 and SP-200 in MilliQ water, the mean particle sizes were approximately 48 nm, 99 nm, and 176 nm, respectively (Table 1), which agreed well with the nominal diameters as stated by the supplier. The ζ-potentials of the silica particles ranged from −43.2 to −53.8 mM (Table 1). Then, to investigate how the state of the silica particles changed after oral administration, and during their passage through the gastrointestinal tract, the silica particles were dispersed in various types of simulated fluids. As shown in Fig. 2, when these silica particles were dispersed in fasted- and fed-state simulated gastric fluids (FaSSGF and FeSSGF) and fasted-state simulated intestinal fluids (FaSSIF), the mean particle sizes of SP-50, SP-100, and SP-200 were not affected. By contrast, when the silica particles were dispersed in fed-state simulated intestinal fluids (FeSSIF), the mean measured particle sizes of SP-50, SP-100, and SP-200 all significantly increased, to more than 1000 nm (Fig. 2). In addition, the PDI values of the silica particles dispersed in FeSSIF also increased to approximately 0.6, indicating that the SP-50, SP-100, and SP-200 particles all agglomerated in FeSSIF, regardless of the primary particle size. Then, to investigate conditions more similar to those encountered in actual oral administration before the passage through the intestinal tract, the silica particles were first diluted with simulated gastric fluids; this was then followed by dispersion in simulated intestinal fluids. As shown in Fig. 2, when the silica particles were dispersed in fasted-state simulated fluids (FaSSGF and FaSSIF), the mean particle sizes of SP-50, SP-100, and SP-200 were not affected. By contrast, when SP-50, SP-100, and SP-200 were dispersed in fed-state simulated fluids (FeSSGF and FeSSIF), the mean measured particle sizes increased to more than 1000 nm (Fig. 2). These results suggested that silica particles—at least those used in this study—would agglomerate after postprandial oral administration.

3.2. Stability of fluorescent labeling of silica particles

The intracellular uptake and transcellular transport assay of silica particles depend on the accuracy of the measured fluorescence. The studies supporting stability of fluorescent labeling were performed. After incubation of fluorescently labeled silica particles in various fluids, the recovery of fluorescent dye was examined. As shown in Table 3, the fluorescent labeling of silica particles used in this study was stable in every fluid under the conditions used in this study.

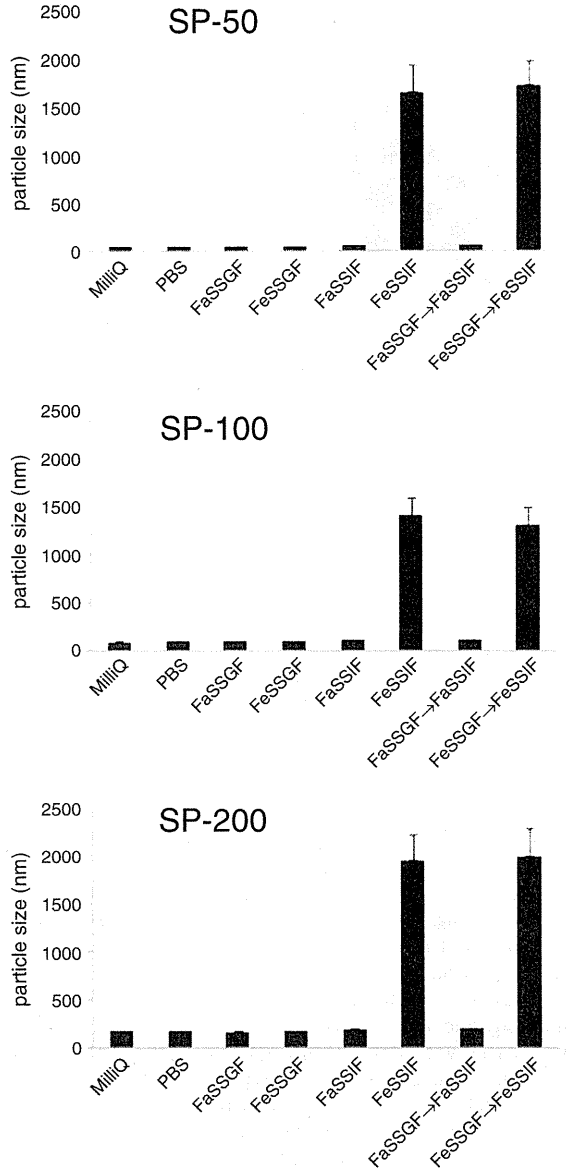

Fig. 2. Sizes of amorphous silica particles (SP-50, 100, and 200, 0.1 mg/mL) in various types of fluids. The mean particle size of the silica particles was measured using a Zetasizer Nano-ZS (Malvern Instruments, UK), with a concentration of 0.1 mg/mL. Each value represents the mean + S.D. ($n = 3$).

3.3. Effects of simulated gastric and intestinal fluids on the intracellular uptake of fluorescently labeled silica particles

The effects of dispersion in simulated fluids on the intracellular uptake of silica particles were investigated using Caco-2 cells. In the preliminary experiments, we confirmed that the internalization occur linearly with times around 2 h after the addition of silica particles (Supplementary Fig. 1). Therefore, the intracellular amounts of silica particles were measured after incubation for 2 h with silica particles. Similarly, the silica particle concentrations for incubation were determined based on the linearity between silica particle masses and fluorescent intensities of internalized silica particles (Supplementary Fig. 2). As shown in Fig. 3, the intracellular amounts of SP-50, SP-100, and SP-200 dispersed in fasted-state simulated fluids (FaSSGF and FaSSIF) were almost the same as those in cultured medium (control). However, when SP-50, SP-100, and SP-200 were dispersed in fed-state simulated

Table 3
Stability of fluorescent labeling.

Solution	SP-50	SP-100	SP-200
	Average SD	Average SD	Average SD
MilliQ water	97.8 ± 0.62	99.8 ± 1.40	98.5 ± 4.18
PBS	98.2 ± 1.06	99.3 ± 1.05	98.9 ± 3.55
D-MEM(+)	98.8 ± 0.91	99.5 ± 1.04	98.2 ± 3.34
FaSSIF	99.1 ± 0.53	99.8 ± 1.00	98.4 ± 3.48
FeSSIF	98.4 ± 0.37	99.1 ± 0.68	98.5 ± 2.30
FaSSGF	98.4 ± 0.73	99.0 ± 0.49	98.1 ± 2.56
FeSSGF	97.6 ± 0.61	99.1 ± 0.37	98.5 ± 1.61
Trypsin	98.5 ± 5.90	98.3 ± 7.49	99.9 ± 11.2
Lysis buffer	101.5 ± 5.76	103.8 ± 6.29	99.9 ± 8.63

After incubation of fluorescent labeled silica particles in various solutions, the recovery of fluorescent dye was examined and expressed as percentage of the fluorescent intensity of the resuspended silica particles to that before centrifugation as described in "Materials and methods." Each value represents the mean ± S.D. ($n = 3$).

intestinal fluids (FeSSIF), the measured amounts of intracellular silica particles significantly decreased (Fig. 3). This decrease in the intracellular amounts of silica particles was also observed when the silica particles were serially diluted using FeSSGF and FeSSIF (Fig. 3). We then examined the intracellular uptake of silica particles into Caco-2 cells using confocal microscopy. As shown in Fig. 4 (a), when silica particles were pre-incubated in fasted-state simulated fluids (FaSSIF), the intracellular uptake of silica particles was almost the same as that in PBS. In contrast, when silica particles were pre-incubated in fed-state simulated intestinal fluids (FeSSIF), the intracellular uptake of silica particles significantly decreased (Fig. 4 (a)). This result agreed with the quantitative values obtained using fluorescent spectroscopy described above (Fig. 3). It was also shown that silica particles pre-incubated in PBS and FaSSIF were observed to co-localize with endosomes and lysosomes after incubation for 2 h with Caco-2 cells (Fig. 4 (a)). On the other hand, the internalization of silica particles was not observed when the particles were incubated with Caco-2 cells at 4 °C (Fig. 4 (b)). These indicated that the silica particles were internalized by endocytosis, and that the silica nanoparticles are not simply adhering to the cells.

3.4. Effects of simulated gastric and intestinal fluids on the Caco-2 cell monolayer transport of silica particles

To investigate the effect of various fluids on the transcellular transport of silica particles, SP-50, SP-100, and SP-200 were dispersed in PBS, FaSSIF, and FeSSIF, and silica particle transport studies were performed using Caco-2 cell monolayers (Fig. 5). Fig. 6 shows the time-dependent variations in the TEER and the cumulative amount of transported silica particles dispersed in various types of fluids. The TEER is well known as an indicator of the integrity, or tightness, of junctions (a tight junction is described as the closely associated area between two cells whose membranes have joined together to form a virtually impermeable barrier against various materials) [25]. As shown in Fig. 6, the TEER was hardly affected by the addition of SP-50, SP-100, or SP-200 under these experimental conditions, suggesting that the silica particles used in this study did not significantly change the structure of the tight junctions in the Caco-2 cell monolayers. From the investigation of the cumulative amounts of transported silica particles, it was clear that after 30 min, the transported amounts of SP-50 suspended in PBS and fasted-state fluid were significantly higher than those of SP-50 in fed-state fluid. The transported amounts of SP-50 dispersed in FeSSIF were significantly lower than those of SP-50 dispersed in PBS or fasted-state fluids. In the case of SP-100 and SP-200, the cumulative amount of transported silica particles was negligible until 60 min, even in the PBS and fasted-state fluids (Fig. 6).

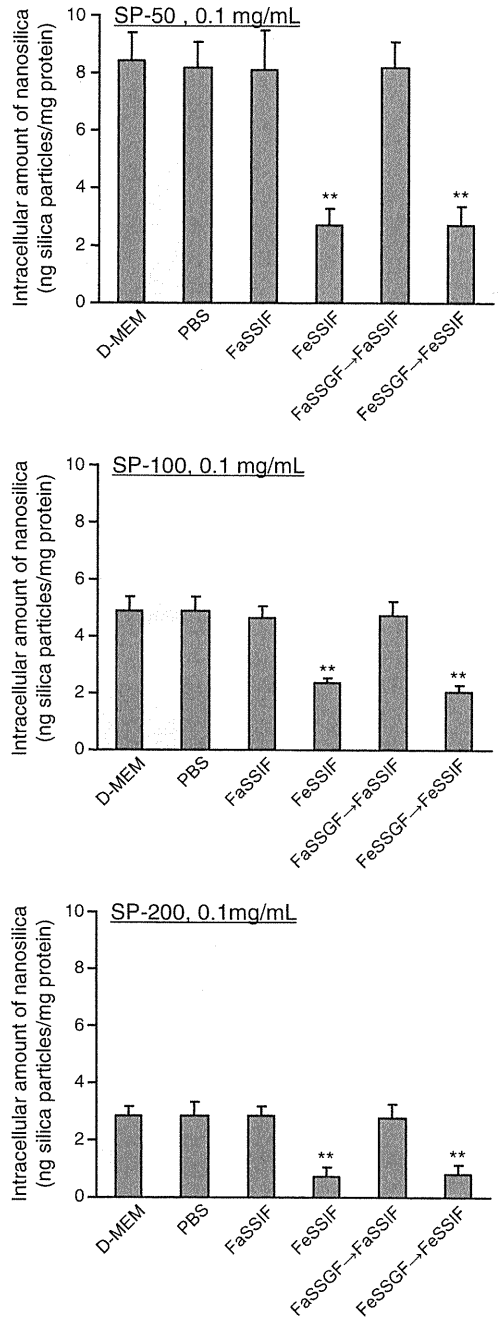

**P<0.01, compared with the corresponding group of D-MEM.

Fig. 3. The intracellular uptake of amorphous silica particles, 2 h after their addition to Caco-2 cells. SP-50, SP-100, and SP-200 were dispersed in various types of fluids and pre-incubated for 1 h. After incubation for 2 h in the silica particle-containing suspension, the cells were then trypsinized, washed, and lysed. The cell suspension was shaken, centrifuged, and the fluorescence intensity of the resulting supernatant was measured as described in Section 2.5. $^{**}P < 0.01$, compared with the corresponding group of D-MEM. Each value represents the mean + S.D. ($n = 6$).

3.5. Effects of simulated gastric and intestinal fluids on the cytotoxicity of silica particles

The effects of various fluids on the cytotoxicity of the silica particles were then evaluated. Silica nanoparticles (final concentration 1.0 mg/mL) were dispersed in various types of fluids and exposed to cells for

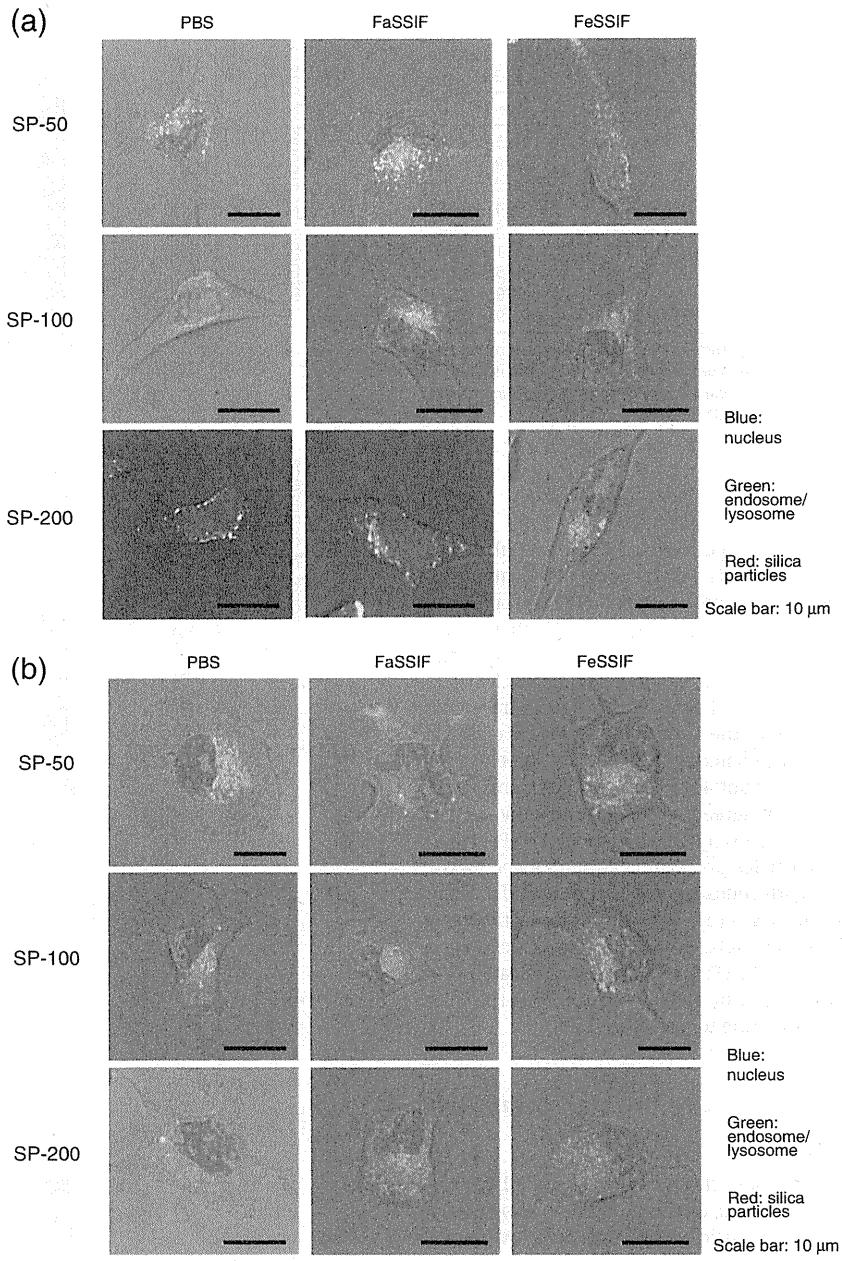

Fig. 4. Confocal images of the intracellular amorphous silica particles, taken 2 h after their addition to Caco-2 cells. The fluorescently labeled silica particles were diluted to a concentration of 0.1 mg/mL in various types of fluids (PBS, FaSSIF, and FeSSIF), and pre-incubated for 1 h to mimic the intestinal conditions. Confocal images of the intracellular amorphous silica particles were taken 2 h after their addition to Caco-2 cells at 37 °C (a) or 4 °C (b). To observe co-localization, endosomes and lysosomes of cells were labeled with AlexaFluor-488-conjugated transferrin and LysoTracker Green DND-26, respectively. The scale bars represent 10 μm.

6 h. Up to this time point, no cytotoxicity was observed in Caco-2 cells exposed to SP-50, SP-100, or SP-200. The cultured media was then replaced with fresh medium without silica particles to eliminate any effect of the fluid itself, and the cells were incubated for another 0, 6, 24, and 48 h (Fig. 7). During this additional incubation with fresh medium, time-dependent toxicity was observed in Caco-2 cells that had been initially exposed to SP-50 dispersed in PBS or fasted-state simulated fluids. By contrast, no cytotoxicity was observed for SP-100 or SP-200 even after 48-h incubation (Fig. 7). We then investigated the concentration dependency of the silica particle toxicity on Caco-2 cells. Silica nanoparticles (final concentration 0.1, 1.0, and 10 mg/mL) were dispersed in various types of fluids and exposed to cells for 6 h. The cultured media was then replaced with fresh medium without silica particles, and the cells were incubated for another 48 h at which time the cytotoxicity of SP-50 was considerable (Fig. 7). As shown in Fig. 8, cytotoxicity was not observed for SP-100 or SP-200 in any of the various types of fluids, even at a concentration of 10 mg/mL. By contrast, when SP-50 was dispersed in PBS or the fasted-state simulated fluids, significant cytotoxicity was detected for all concentrations of the particles, with the cytotoxicity depending on the concentration. However, when SP-50 was dispersed in FeSSIF, cytotoxicity was not observed.

4. Discussion

With the increasing interest in nanotechnology, nanomaterials have been applied in various fields including medicines. Nanoparticles can

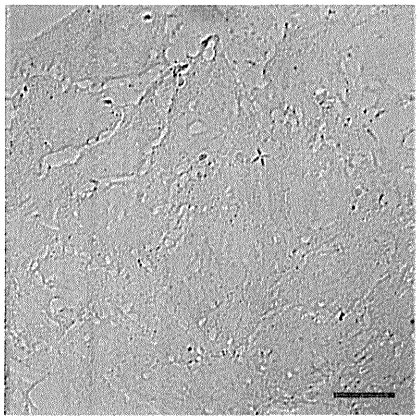

Fig. 5. Phase-contrast image of the Caco-2-cells. The scale bar represents 20 μm.

also be used as excipients of solid oral dosage forms and other products that are absorbed in a body in a variety of ways.

In solid oral dosage form, silicates are commonly used as glidants. Although the primary particle size of the most frequently used colloidal silica (Aerosil 200) is between 7 and 40 nm, these particles group together into so-called aggregates of a few hundred nanometers during the sintering production process [26]. This study therefore investigated the size and in vitro behavior using gastrointestinal models; the Caco-2 cell models and bio-relevant dissolution media simulated conditions in the gastrointestinal system, allowing an evaluation of the intestinal permeability properties and the intestinal cell toxicity associated with oral administration. The critical question regarding the safety of oral dosage forms is whether the material used as an excipient will penetrate the intestinal barrier of the intestinal membrane.

We used fluorescently labeled silica particles to trace the intake and the translocation of the intestinal barrier. The silica particles consisted of amorphous and nonporous silicates, and had a negative charge (Table 1); these characteristics are the same as those of silicates frequently used in solid oral dosage form (approximately −40 mV in

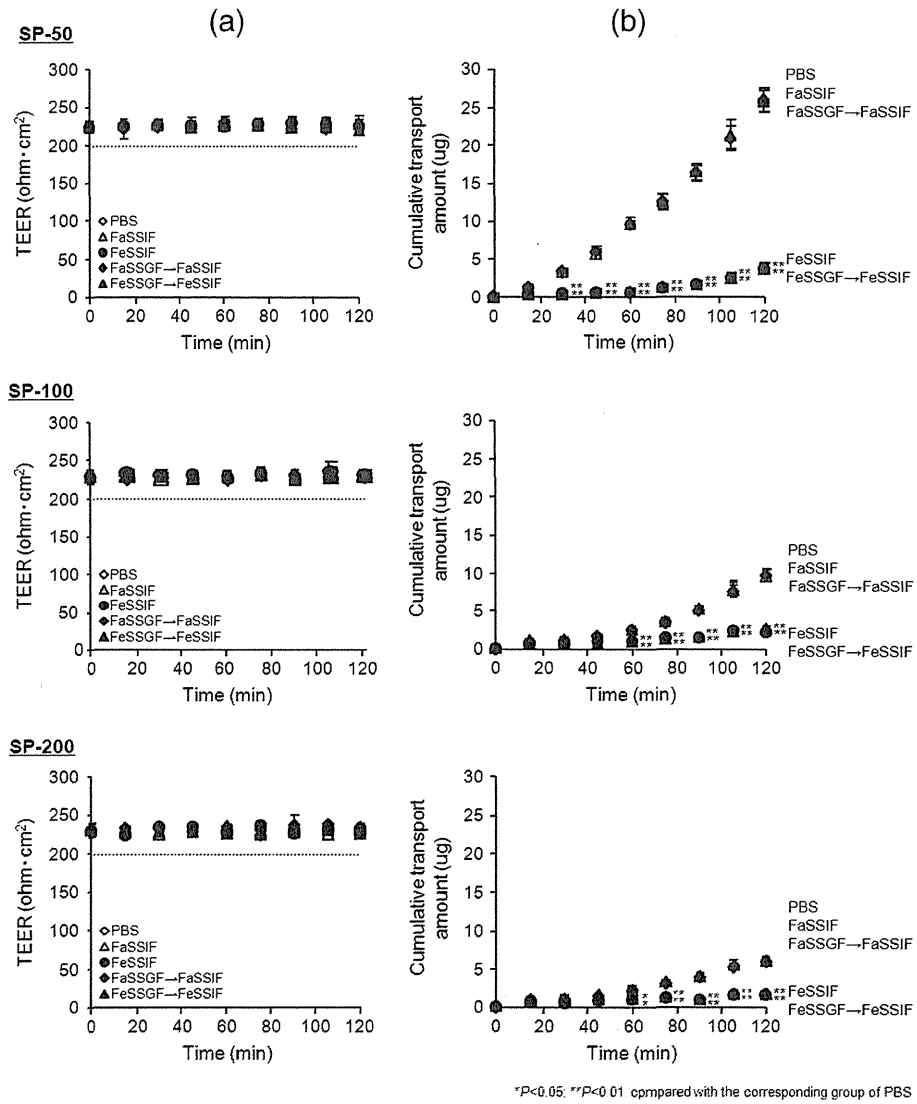

Fig. 6. Trans-epithelial electrical resistance across Caco-2 cell monolayers (a), and cumulative transported amounts of amorphous silica particles (b). SP-50, SP-100, and SP-200 were dispersed in various types of fluids to a final concentration of 1 mg/mL and pre-incubated at 37 °C for 1 h. The incubated fluorescently labeled silica particles were added to the apical side of the Caco-2 cell monolayer. After indicated duration, TEER and the transported amount of nanoparticles were measured as described in "Materials and methods". $^{*}P < 0.05$, $^{**}P < 0.01$, compared with the corresponding group of " PBS". Each value represents the mean ± S.D. ($n = 4$).

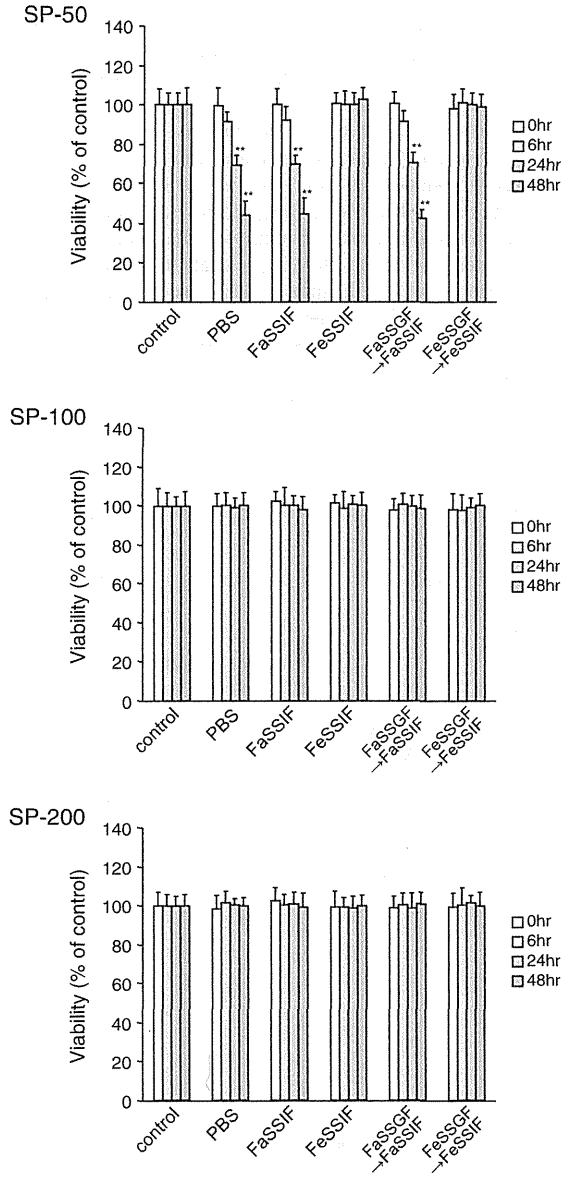

Fig. 7. The cytotoxicity of amorphous silica particles against Caco-2 cells. Silica nanoparticles (final concentration 1.0 mg/mL) were dispersed in various types of fluids and pre-incubated at 37 °C for 1 h. In addition, to mimic the gastric and intestinal conditions (indicated as "FaSSGF → FaSSIF" and "FeSSGF → FeSSIF"), silica particles were diluted to 10 mg/mL in FaSSGF or FeSSGF, incubated at 37 °C for 1 h, and the diluted silica particles were subsequently further diluted to concentrations of 1.0 mg/mL in FaSSIF or FeSSIF, and incubated at 37 °C for an additional 1 h. The pre-incubated particles were added to the cells. After incubation for 6 h, the cultured media was then replaced with fresh medium to eliminate the effect of the fluid itself, and the cells were incubated for another 0, 6, 24, and 48 h. Cell viability was evaluated by using the WST-8 assay at each time point (0, 6, 24, and 48 h). $^{**}P < 0.01$, compared with the corresponding control group. Each value represents the mean ± S.D. ($n = 4$).

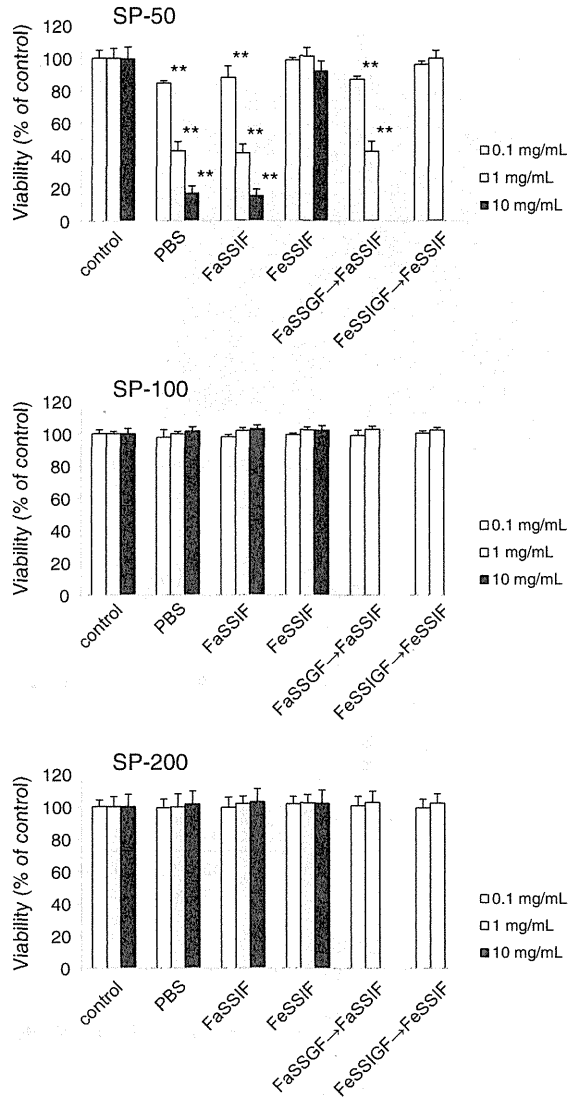

Fig. 8. The concentration dependency of the silica particle toxicity on Caco-2 cells. SP-50, SP-100, and SP-200 (final concentration 0.1, 1.0, and 10 mg/mL) were dispersed in various types of fluids and pre-incubated at 37 °C for 1 h. In addition, to mimic the gastric and intestinal conditions (indicated as "FaSSGF → FaSSIF" and "FeSSGF → FeSSIF"), silica particles were diluted to 10 mg/mL in FaSSGF or FeSSGF, incubated at 37 °C for 1 h, and the diluted silica particles were subsequently further diluted to concentrations of 0.1 or 1.0 mg/mL in FaSSIF or FeSSIF, and incubated at 37 °C for an additional 1 h. The pre-incubated particles were added to the cells. After incubation for 6 h, the cultured media was then replaced with fresh medium to eliminate the effect of the fluid itself, and an additional 48 h of incubation was applied, followed by measurement of cytotoxicity. $^{**}P < 0.01$, compared with the corresponding control group. Each value represents the mean ± S.D. ($n = 4$).

water at pH 7 [27]). We also investigated the size dependence of the absorption and the in vitro toxicity, using silica particles with diameters of 50, 100, and 200 nm.

First, we investigated whether the silica particles would agglomerate after oral administration. Simulation of gastrointestinal conditions is essential to adequately predict the in vivo behavior of drug formulations. We used biorelevant dissolution media that can be used for the in vitro simulation of different dosing conditions (fasted and fed states) [28]. Regardless of the primary particle size, the observed tendency was the same. In all cases, the particles formed agglomerates in the medium representing the fed-state intestinal fluid. It is known that acidic conditions promote agglomeration, due to a decrease in the electrostatic repulsion between negatively charged silica particles; the formation of agglomerates can therefore occur after passage through the stomach, which has lower-pH conditions. However, in this case, lower-pH conditions did not cause agglomeration, under fed or fasted conditions. Furthermore, the viscosity of the FaSSGF = 0.688 mPa s and FeSSGF = 0.704 mPa s were almost the same, which suggested that the viscosity did not affect the agglomeration of the silica particles. Judging from the composition of the bio-relevant dissolution media, and the above results, we concluded that the high salt concentration was a major factor causing the agglomeration. In fact, we reported previously

that silica particles easily agglomerated with high sodium ion concentrations in solution eluents [29], and the same phenomenon was also reported by other researchers [30]. The Derjaguin Landau_Verwey_Overbeek (DLVO) theory is often used to explain the aggregation/agglomeration behavior of silica suspensions [31,32]. Briefly, the DLVO theory combines the effects of the attractive van der Waals forces and the electrostatic repulsion between charged surfaces. As discussed earlier, the presence of silanol groups (Si–O–H) on amorphous silica surfaces and the charge of silanol groups determine the extent of the repulsive energy needed to keep the silica nanoparticles dispersed. The surface charge of silica nanoparticles differs as the pH changes due to protonation and deprotonation of the silanol groups. At pH 2–3, silica nanoparticles reach the isoelectric point (IEP) where the particles carry no net charge, causing the nanoparticles to agglomerate. In the case of biological conditions with high (0.1–0.3 M) salt concentrations, ion-specific effects also play a prominent role [33]. Amiri et al. pointed out that in aqueous media, because pure particles are electrostatically stabilized, interparticle interactions at a given concentrations can be changed by varying the ionic strength, particle size, and pH of the suspension; they demonstrated that high salt concentration causes agglomeration of silica particles [27].

Next, we studied the cellular uptake of silica particles, using Caco-2 cells as an in vitro model to assess the barrier integrity/permeability effects of the silica particles. The TEER, which is well known as an indicator of the integrity of junctions, was not affected by the addition of SP-50, SP-100, or SP-200 under these experimental conditions, suggesting that the silica particles used in this study did not significantly change the structure of the tight junctions between the cells in the Caco-2 cell monolayer, regardless of the particle size, at least for 2 h of exposure to the particles. Because the length of the tight junction between the cells is approximately 10–20 nm [25], the silica particles used in this study did not penetrate the junction. Therefore, the increase in the amount of particles showed that translocation through the Caco-2 cells occurred. The transport experiments showed that the cumulative number of transported silica particles increased with exposure time, and it is notable that translocation occurred under conditions that did not cause agglomeration. In the investigation of the cumulative amount of transported silica particles, Fig. 6 showed that the transported amounts of SP-50 were much higher than those of SP-100 and 200 when these silica particles were dispersed in PBS and FaSSIF. Moreover, the transported amounts of all of the silica particles were significantly lower when they were dispersed in FeSSIF than when they were dispersed in PBS or FaSSIF. However, in the case of SP-100 and SP-200, the amounts of silica particles transported were negligible for times shorter than 1 h, regardless of which fluid was used. Because the transit time in the gut is approximately 1 h per 1 m of gut length [34], these results suggest that the intestinal absorption of silica particles or aggregates/agglomerates larger than 100 nm would be negligible. Further in vivo testing would be necessary to confirm the possibility of silica particle absorption into the systemic circulation.

We then investigated the cytotoxicity of the silica particles towards Caco-2 cells. We confirmed that the exposure for 6 h to the silica particles (SP-50,100, and 200) did not induce cytotoxicity in any of the various types of fluids, and this coincides with our results that the structure of the tight junctions of Caco-2 monolayer was not changed at least for 2 h of exposure to the silica particles (Fig. 6). However, after another incubation with fresh medium, SP-50 showed time-dependent toxicity for up to 48 h when SP-50 was dispersed in PBS or fasted-state simulated fluids. On the other hand, SP-100 and SP-200 did not show any cytotoxicity, at least for 48 h (Fig. 7). The time lapse of toxicity observed in SP-50 in this study indicates that the smaller size of silica particles inhibited cellular proliferation, which has also been reported by Nabeshi et al. [35]. They showed the size-dependent cytotoxic effects of amorphous silica particles (70, 300, and 1000 nm) on mouse epidermal Langerhans cells. The smallest particles induced greater cytotoxicity and inhibited cellular proliferation [35]. We investigated the concentration dependency of silica particles on Caco-2 cells and found that SP-50 was cytotoxic. No cytotoxicity was observed, however, for SP-100 or SP-200, in any of the various types of fluids, even at a concentration of 10 mg/mL (Fig. 8). By contrast, when SP-50 was dispersed in PBS or fasted-state simulated fluids, significant cytotoxicity was detected for all concentrations of the particles, with increasing cytotoxicity as the silica concentration increased. Although SP-100 and 200 were also internalized in the Caco-2 cells in the fasted state, cytotoxicity was not observed.

The size-dependent toxicity of amorphous nanosilica has been also reported by other researchers [16]. The relationship between cytotoxicity and particle sizes observed in our study has been discussed previously by others. Yu et al. examined the cytotoxic activity of well-dispersed amorphous silica particles (30–535 nm) in mouse keratinocytes [36]. All sizes of particles were taken up into the cell cytoplasm. The toxicity was dose- and size-dependent, with 30- and 48-nm particles being more cytotoxic than 118- and 535-nm particles. Nabeshi et al. showed the size-dependent cytotoxic effects of amorphous silica particles (70, 300, and 1000 nm) on mouse epidermal Langerhans cells [35]. They found that the smallest particles induced the greatest cytotoxicity and inhibited cellular proliferation. These observed effects were associated with the quantity of particle uptake into the cells. This association was also present in our study, where the cytotoxicity of SP-50 correlated with the concentration (Fig. 8). Yang et al. evaluated the effects of amorphous silica particles (15 and 30 nm) on cellular viability, the cell cycle, and apoptosis in the human epidermal keratinocyte cell line HaCaT [37]. Their microscopic examination revealed morphological changes after 24-h exposures. Cell growth also appeared to be significant inhibited, and the smaller silica particles were more cytotoxic and induced a higher rate of apoptosis. Oberdörster et al. argued that since smaller particles have a bigger surface area per unit of mass, the surface area is a pivotal factor for the displayed biological activity [38]. The mechanisms by which silica particles exert their cytotoxic effects are still largely unknown, and recent research illustrates the complexity in identifying the hazards of nanoparticles for human health [39]. However, there are many possibilities, including damage to the plasma membrane before particles penetrate the cells, intracellular interference after uptake in late or lysosomal structures, and lysosomal escape [16]. Another research indicated that the effect of silica nanoparticles on HT-29 cells is mediated by the interference with the signaling pathway such as MAPK/ERK1/2 [40].

Our study showed that when SP-50 was dispersed in FeSSIF, large agglomerates were formed, and cytotoxicity was not observed. This indicated that even if the primary particle size was less than 100 nm, the cytotoxicity was largely affected by the agglomerate formation.

Guidance for the assessment of risks associated with the application of nanoscience and nanotechnologies in the food and feed chain [41] recommends in vitro tests, including assessments of the effect of particles on the integrity of the gastrointestinal barriers. Our studies proposed one model to assess the integrity/permeability of the gastrointestinal barrier, and the cytotoxicity based on differentiated Caco-2 cells. Parameters such as the cell viability and the TEER can be also considered to be recommended in the guidance.

5. Conclusions

In the present study, we developed the in vitro assay systems including cellular uptake, transport study, and cytotoxicity study models using Caco-2 cells and simulated gastrointestinal fluids to help the evaluation of the intestinal permeability properties and intestinal cell toxicity of silica particles after they were administered orally. Our study showed that the agglomeration of silica particles was affected by the diet and gastrointestinal fluids. Our study also indicated that there was no significant penetration of silica particles through in vitro models (Caco-2 cells), and the cytotoxicity was not observed if the mean size was larger than 100 nm. This study further showed that the secondary size, including

the factor of agglomeration, is important to assess the potential harmful effects of silica particles on Caco-2 cells. Even when the primary particle size was less than 100 nm, the cytotoxicity was affected by agglomerate formation. The findings obtained from our study may offer valuable information to evaluate the behavior in the gastrointestinal tracts or safety of medicines or foods containing silica particles as additives.

Supplementary data to this article can be found online at http://dx.doi.org/10.1016/j.bbagen.2013.12.014.

Acknowledgement

This work was supported in part by the Health and Labour Sciences Research Grants from the Ministry of Health, Labour and Welfare of Japan.

References

[1] A.B. Lansdown, A. Taylor, Zinc and titanium oxides: promising UV-absorbers but what influence do they have on the intact skin? Int. J. Cosmet. Sci. 19 (1997) 167–172.
[2] H. Nabeshi, T. Yoshikawa, K. Matsuyama, Y. Nakazato, K. Matsuo, A. Arimori, M. Isobe, S. Tochigi, S. Kondoh, T. Hirai, T. Akase, T. Yamashita, K. Yamashita, T. Yoshida, K. Nagano, Y. Abe, Y. Yoshioka, H. Kamada, T. Imazawa, N. Itoh, S. Nakagawa, T. Mayumi, S. Tsunoda, Y. Tsutsumi, Systemic distribution, nuclear entry, and cytotoxicity of amorphous nanosilica following topical application, Biomaterials 32 (2011) 2713–2724.
[3] A. Kunzmann, B. Andersson, T. Thurnherr, H. Krug, A. Scheynius, B. Fadeel, Toxicology of engineered nanomaterials: focus on biocompatibility, biodistribution, and biodegradation, Biochim. Biophys. Acta 1810 (2011) 361–373.
[4] A.M. Nyström, B. Fadeel, Safety assessment of nanomaterials: implications for nanomedicine, J. Control. Release 161 (2012) 403–408.
[5] M. Ferrari, Cancer nanotechnology: opportunities and challenges, Nat. Rev. Cancer 5 (2005) 161–171.
[6] Y. Malam, M. Loizidou, A.M. Seifalian, Liposomes and nanoparticles: nanosized vehicles for drug delivery in cancer, Trends Pharmacol. Sci. 30 (2009) 592–599.
[7] N. Nishiyama, K. Kataoka, Current state, achievements, and future prospects of polymeric micelles as nanocarriers for drug and gene delivery, Pharmacol. Ther. 112 (2006) 630–648.
[8] R.A. Petros, J.M. DeSimone, Strategies in the design of nanoparticles for therapeutic applications, Nat. Rev. Drug Discov. 9 (2010) 615–627.
[9] C.M. Hentzschel, M. Alnaief, I. Smirnova, A. Sakmann, C.S. Leopold, Tableting properties of silica aerogel and other silicates, Drug Dev. Ind. Pharm. 38 (2012) 462–467.
[10] L. Jia, J. Shen, Z. Li, D. Zhang, Q. Zhang, G. Liu, D. Zheng, X. Tian, In vitro and in vivo evaluation of paclitaxel-loaded mesoporous silica nanoparticles with three pore sizes, Int. J. Pharm. 445 (2013) 12–19.
[11] H. Miura, M. Kanebako, H. Shirai, H. Nakao, T. Inagi, K. Terada, Influence of particle design on oral absorption of poorly water-soluble drug in a silica particle–supercritical fluid system, Chem. Pharm. Bull. 59 (2011) 686–691.
[12] M.D. Popova, A. Szegedi, I.N. Kolev, J. Mihaly, B.S. Tzankov, G.T. Momekov, N.G. Lambov, K.P. Yoncheva, Carboxylic modified spherical mesoporous silicas as drug delivery carriers, Int. J. Pharm. 436 (2012) 778–785.
[13] P.J. Borm, D. Robbins, S. Haubold, T. Kuhlbusch, H. Fissan, K. Donaldson, R. Schins, V. Stone, W. Kreyling, J. Lademann, J. Krutmann, D. Warheit, E. Oberdorster, The potential risks of nanomaterials: a review carried out for ECETOC, Part. Fibre Toxicol. 3 (2006) 11.
[14] K.M. Waters, L.M. Masiello, R.C. Zangar, B.J. Tarasevich, N.J. Karin, R.D. Quesenberry, S. Bandyopadhyay, J.G. Teeguarden, J.G. Pounds, B.D. Thrall, Macrophage responses to silica nanoparticles are highly conserved across particle sizes, Toxicol. Sci. 107 (2009) 553–569.
[15] T. Hirai, T. Yoshikawa, H. Nabeshi, T. Yoshida, S. Tochigi, K. Ichihashi, M. Uji, T. Akase, K. Nagano, Y. Abe, H.K. amada, N. Itoh, S. Tsunoda, Y. Yoshioka, Y. Tsutsumi, Amorphous silica nanoparticles size-dependently aggravate atopic dermatitis-like skin lesions following an intradermal injection, Part. Fibre Toxicol. 9 (2012) 3.
[16] J. Kasper, M.I. Hermanns, C. Bantz, O. Koshkina, T. Lang, M. Maskos, C. Pohl, R.E. Unger, C.J. Kirkpatrick, Interactions of silica nanoparticles with lung epithelial cells and the association to flotillins, Arch. Toxicol. 87 (2012) 1053–1065.
[17] M. Pinto, S. Robine-Leon, M.D. Appay, M. Kedinger, N. Triadou, I. Dussaulx, B. Lacroix, P. Simon-Assmann, K. Haffen, J. Fogh, A. Zweibaum, Enterocyte-like differentiation and polarization of the human colon carcinoma cell line Caco-2 in culture, Biol. Cell 47 (1983) 323–330.
[18] I.J. Hidalgo, T.J. Raub, R.T. Borchardt, Characterization of the human colon carcinoma cell line (Caco-2) as a model system for intestinal epithelial permeability, Gastroenterology 96 (1989) 736–749.
[19] P. Artursson, J. Karlsson, Correlation between oral drug absorption in humans and apparent drug permeability coefficients in human intestinal epithelial (Caco-2) cells, Biochem. Biophys. Res. Commun. 175 (1991) 880–885.
[20] K. Gerloff, C. Albrecht, A.W. Boots, I. Forster, R.P.F. Schins, Cytotoxicity and oxidative DNA damage by nanoparticles in human intestinal Caco-2 cells, Nanotoxicology 3 (2009) 355–364.
[21] N. Reix, A. Parat, E. Seyfritz, R. Van der Werf, V. Epure, N. Ebel, L. Danicher, E. Marchioni, N. Jeandidier, M. Pinget, Y. Frere, S. Sigrist, In vitro uptake evaluation in Caco-2 cells and in vivo results in diabetic rats of insulin-loaded PLGA nanoparticles, Int. J. Pharm. 437 (2012) 213–220.
[22] V. Uskoković, K. Lee, P.P. Lee, K.E. Fischer, T.A. Desai, Shape effect in the design of nanowire-coated microparticles as transepithelial drug delivery devices, ACS Nano 6 (2012) 7832–7841.
[23] E. Jantratid, N. Janssen, C. Reppas, J.B. Dressman, Dissolution media simulating conditions in the proximal human gastrointestinal tract: an update, Pharm. Res. 25 (2008) 1663–1676.
[24] V.G. DeMarco, N. Li, J. Thomas, C.M. West, J. Neu, Glutamine and barrier function in cultured Caco-2 epithelial cell monolayers, J. Nutr. 133 (2003) 2176–2179.
[25] J.M. Anderson, Molecular structure of tight junctions and their role in epithelial transport, News Physiol. Sci. 16 (2001) 126–130.
[26] Evonik Industries: Technical Information No. 1271.
[27] A. Amiri, G. Oye, J. Sjoblom, Influence of pH, high salinity, and particle concentration on stability and rheological properties of aqueous suspensions of fumed silica, Colloids Surf. A Physicochem. Eng. Asp. 349 (2009) 43–54.
[28] S. Klein, The use of biorelevant dissolution media to forecast the in vivo performance of a drug, AAPS J. 12 (2010) 397–406.
[29] K. Sakai-Kato, S. Ota, T. Takeuchi, T. Kawanishi, Size separation of colloidally dispersed nanoparticles using a monolithic capillary column, J. Chromatogr. A 1218 (2011) 5520–5526.
[30] J. Depasse, A. Watillon, The stability of amorphous colloidal silica, J. Colloid Interface Sci. 33 (1970) 430–438.
[31] E.J.W. Verwey, J.T.G. Overbeek, Theory of the Stability of Lyophobic Colloids, Elsevier, Amsterdam, 1948.
[32] B. Derjaguin, L. Landau, Theory of the stability of strongly charged lyophobic sols and of the adhesion of strongly charged particles in solution of electrolytes, Acta Phys.-Chim. 14 (1941) 633–662(URSS).
[33] R. Peters, E. Kramer, A.G. Oomen, Z.E. Rivera, G. Oegema, P.C. Tromp, R. Fokkink, A. Rietveld, H.J. Marvin, S. Weigel, A.A. Peijnenburg, H. Bouwmeester, Presence of nano-sized silica during in vitro digestion of foods containing silica as a food additive, ACS Nano 6 (2012) 2441–2451.
[34] N. Parrott, V. Lukacova, G. Fraczkiewicz, M.B. Bolger, Predicting pharmacokinetics of drugs using physiologically based modeling-application to food effects, AAPS J. 11 (2009) 45–53.
[35] H. Nabeshi, T. Yoshikawa, K. Matsuyama, Y. Nakazato, A. Arimori, M. Isobe, S. Tochigi, S. Kondoh, T. Hirai, T. Akase, T. Yamashita, K. Yamashita, T. Yoshida, K. Nagano, Y. Abe, Y. Yoshioka, H. Kamada, T. Imazawa, N. Itoh, S. Tsunoda, Y. Tsutsumi, Size-dependent cytotoxic effects of amorphous silica nanoparticles on Langerhans cells, Pharmazie 65 (2010) 199–201.
[36] K.O. Yu, C.M. Grabinski, A.M. Schrand, R.C. Murdock, W. Wang, B. Gu, J.J. Schlager, S.M. Hussain, Toxicity of amorphous silica nanoparticles in mouse keratinocytes, J. Nanopart. Res. 11 (2009) 15–24.
[37] X. Yang, J. Liu, H. He, L. Zhou, C. Gong, X. Wang, L. Yang, J. Yuan, H. Huang, L. He, B. Zhang, Z. Zhuang, SiO2 nanoparticles induce cytotoxicity and protein expression alteration in HaCaT cells, Part. Fibre Toxicol. 7 (2010) 1–12.
[38] G. Oberdörster, E. Oberdörster, J. Oberdörster, Nanotoxicology: an emerging discipline evolving from studies of ultrafine particles, Environ. Health Perspect. 113 (2005) 823–839.
[39] J.A. Sergent, V. Paget, S. Chevillard, Toxicity and genotoxicity of nano-SiO2 on human epithelial intestinal HT-29 cell line, Ann. Occup. Hyg. 56 (2012) 622–630.
[40] H. Gehrke, A. Frühmesser, J. Pelka, M. Esselen, L.L. Hecht, H. Blank, H.P. Schuchmann, D. Gerthsen, C. Marquardt, S. Diabaté, C. Weiss, D. Marko, In vitro toxicity of amorphous silica nanoparticles in human colon carcinoma cells, Nanotoxicology 7 (2013) 274–293.
[41] EFSA Scientific Committee, Scientific opinion: guidance on the risk assessment of the application of nanoscience and nanotechnologies in the food and feed chain, EFSA J. 9 (2011) 2140.

molecular pharmaceutics

Article

pubs.acs.org/molecularpharmaceutics

Effects of Liposomal Phospholipids and Lipid Transport-Related Protein on the Intracellular Fate of Encapsulated Doxorubicin

Keita Un,[†] Kumiko Sakai-Kato,*[,†] Toru Kawanishi,[‡] Haruhiro Okuda,[‡] and Yukihiro Goda[†]

[†]Division of Drugs, National Institute of Health Sciences, 1-18-1 Kamiyoga, Setagaya-ku, Tokyo 158-8501, Japan

[‡]National Institute of Health Sciences, 1-18-1 Kamiyoga, Setagaya-ku, Tokyo 158-8501, Japan

Supporting Information

ABSTRACT: We have previously reported the intracellular trafficking mechanism of liposomal phospholipids. In the present study, we investigated the effects of liposomal phospholipids on the intracellular trafficking of doxorubicin (DXR). In DXR-encapsulated liposomes, polyethylene glycol (PEG)-modified phospholipids have been widely used as one of the liposomal lipids. First, we investigated the intracellular trafficking mechanism of 1,2-distearoyl-*sn*-glycero-3-phosphocholine (DSPC) and (1,2-distearoyl-*sn*-glycero-3-phosphoethanolamine-*N*-[methoxy-PEG$_{2000}$] (PEG$_{2000}$-DSPE), and demonstrated that the intracellular trafficking pathways of phospholipids changed by PEG modification. Then, we evaluated the effects of liposomal DXR on the intracellular trafficking of liposomal phospholipids. Under the phosphatidylinositol transfer protein (PITP)-suppressing condition by siRNA treatment, the intracellular amounts of DSPC derived from DXR-encapsulated liposomes were larger than that from nonencapsulated liposomes. Moreover, following the effects of liposomal phospholipids on the intracellular amounts of DXR, the intracellular amounts of DXR were increased under the PITP-suppressing condition in DXR-encapsulated liposomes. We showed that intracellular DXR was associated with the complex of PITP and DSPC, and the extracellular efflux of DXR was enhanced by complex formation with PITP and DSPC.

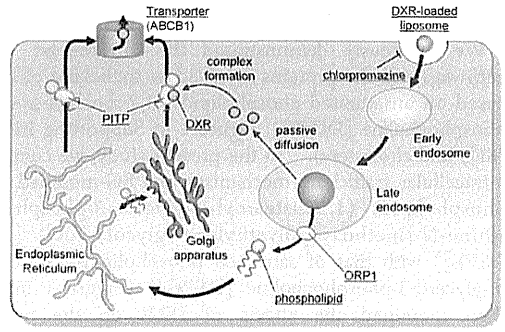

KEYWORDS: *polyethylene glycol-modified liposome, doxorubicin, intracellular trafficking, phosphatidylinositol transfer protein, cytotoxicity*

INTRODUCTION

Liposomes composed of a lipid bilayer membrane are frequently used as membrane models or as drug delivery systems. Because the major components of liposomes are phospholipids and cholesterols, liposomes exhibit low cytotoxicity *in vitro* and *in vivo*.[1] However, their instability *in vivo* and their unexpected uptake into components of the reticuloendothelial system (RES), including the liver and spleen, must be considered when using liposomes.[2] Because of these issues, polyethylene glycol (PEG)-modified liposomes containing PEG-modified phospholipids as functional lipids have been developed.[3,4] The adsorption of complements and serum proteins on PEG-modified liposomes was suppressed by the PEG chain on the surface of liposomes.[5] This modification decreases liposomal uptake into RES and increases the retention time in the blood.[6] Because vascular permeability is greater in tumor tissues than in normal tissues, the accumulation of PEG-modified liposomes in tumor tissue and retention time in the blood were much greater than conventional liposomes.[7] Doxorubicin (DXR)-encapsulated PEG-modified liposomes have already been approved in several countries, and this formulation is expected to be a promising drug with enhanced antitumor activity and reduced side effects compared with conventional DXR.[8,9]

Despite these advantages, the aqueous layer formed by PEG modification suppresses interactions between the liposomes and the cell membrane.[10] Therefore, the intracellular uptake of PEG-modified liposomes into the target cells is less than that of conventional liposomes. Some researchers have successfully developed PEG-modified liposomes in which the PEG chain located on the liposomal surface is selectively cleaved in tumor tissues, enhancing effective intracellular drug delivery.[11,12] On the other hand, to date, there have been very few reports describing the intracellular trafficking mechanism of liposomes containing PEG-modified phospholipids. Our research group has evaluated the intracellular trafficking mechanism of block copolymers including a PEG chain, and showed that this amphipathic polymer was effluxed *via* the ATP-binding cassette transporter (ABC) B1, which is also known as P-glycoprotein (P-gp).[13] Because P-gp is involved in the extracellular efflux of various compounds, including anticancer agents, we thought it was important to determine its role in the intracellular

Received: August 23, 2013
Revised: November 18, 2013
Accepted: January 2, 2014
Published: January 2, 2014

trafficking of PEG-modified phospholipids, a group of amphipathic molecules.

Intracellular trafficking of DXR is generally controlled by passive diffusion. Therefore, there are few reports describing the intracellular trafficking of DXR encapsulated in PEG-modified liposomes. DXR induces the expression of various types of intracellular proteins, including the ABC family of transporters.[14−17] ABC transporters are involved in the extracellular efflux of various drugs and liposomal components, including phospholipids and cholesterols. Therefore, it is important to be able to evaluate and predict the intracellular concentrations of DXR, especially to avoid reducing its pharmacological effects and to minimize unexpected toxicity when using encapsulated formulations of DXR. In this context, improved understanding of the intracellular trafficking of DXR is essential to be able to predict the intracellular concentrations of DXR.

We previously demonstrated the intracellular trafficking pathways and the proteins involved in trafficking of liposomes based on unsaturated phospholipids (1,2-dioleoyl-*sn*-glycero-3-phosphocholine [DOPC], Figure 1 in Supporting Information [SI]) and cholesterol.[18] In the present study, we compared the intracellular trafficking mechanism of PEG-modified saturated phospholipids (1,2-distearoyl-*sn*-glycero-3-phosphoethanolamine-*N*-[methoxy(polyethylene glycol)-2000 [PEG_{2000}-DSPE]) with that of saturated phospholipids (1,2-distearoyl-*sn*-glycero-3-phosphocholine [DSPC]) (Figure 1 in SI). We then examined the effects of DXR on the intracellular trafficking of phospholipids *in vitro*. Finally, we evaluated the effects of liposomal phospholipids on the intracellular trafficking and cytotoxicity of DXR.

EXPERIMENTAL SECTION

Materials and Cells. DSPC and cholesterol (chol) were purchased from Sigma-Aldrich (St. Louis, MO, U.S.A.). PEG_{2000}-DSPE was obtained from NOF (Tokyo, Japan). DXR was purchased from Wako Pure Chemical Industries (Osaka, Japan). Nitrobenzoxadiazol (NBD)-labeled DSPC and carboxyfluorescein (CF)-labeled PEG_{2000}-DSPE were purchased from Avanti Polar Lipids (Alabaster, AL, U.S.A.), and ATTO 647N-labeled 1,2-dioleoyl-*sn*-glycero-3-phosphoethanolamine (DOPE) was obtained from ATTO-TEC (Siegen, Germany). Dulbecco's-modified Eagle's medium (DMEM), penicillin/streptomycin, phosphate-buffer saline (PBS), and Opti-MEM I were purchased from Life Technologies (Brooklyn, NY, U.S.A.). Fetal bovine serum (FBS) was obtained from Nichirei Biosciences (Tokyo, Japan). All other chemicals used in this study were of the highest purity available. HeLa cells (Health Science Research Resources Bank, Osaka, Japan) were cultured in DMEM supplemented with 10% FBS and 100 U/mL penicillin/streptomycin. Cells were grown in a humidified incubator at 37 °C under 5% CO_2.

Preparation of Liposomes. The liposomes used in this study were prepared according to Bangham's method.[19] Briefly, DSPC, chol, and DSPE-PEG_{2000} were mixed in chloroform, and the mixture was dried by evaporation and vacuum desiccated. The resultant lipid film was resuspended in PBS (pH 7.4) or 250 mM ammonium sulfate (pH 5.4) under mechanical agitation. After hydration for 30 min at 65 °C, the dispersion was sonicated for 10 min in a bath-type sonicator (Sharp Manufacturing Systems, Osaka, Japan) and for 3 min in a tip-type sonicator (Sonics, Newtown, CT, U.S.A.). Then, the liposome solution was sized by repeated extrusion through polycarbonate membrane filters (Avestin, Ottawa, ON, Canada) with a pore size of 100 nm. The particle sizes, polydispersity index (PDI), and ζ-potentials of the liposomes were determined using a Zetasizer Nano ZS (Malvern Instrument, Worcestershire, UK). DXR was loaded into liposomes by the remote-loading method.[20] Briefly, the external phase of liposomes hydrated with 250 mM ammonium sulfate (pH 5.4) was replaced with PBS (pH 8.0) by gel filtration using a Sephadex G-25 column (PD-10; GE Healthcare, Buckinghamshire, UK). DXR dissolved in PBS (pH 8.0) was added to the liposome solution at a drug-to-lipid molar ratio of 1:10 and incubated at 60 °C for 1 h.

Evaluation of Intracellular Trafficking of Liposomes. To evaluate the intracellular concentrations of DSPC and PEG_{2000}-DSPE liposomes, we prepared liposomes containing fluorescence-labeled DSPC and PEG_{2000}-DSPE at a molar ratio of 5%. HeLa cells were plated in 12-well plate (2.5×10^4 cells/well) in DMEM containing 10% FBS and 100 U/mL penicillin/streptomycin. After incubation for 48 h (37 °C, 5% CO_2), liposomes were added to the culture medium. After the indicated times, the cells were washed three times in PBS, trypsinized with 0.25% trypsin-ethylenediamine tetraacetic acid (EDTA) (Life Technologies), washed three times with Hanks' balanced salt solution (HBSS) (Life Technologies), and suspended in lysis buffer (1% Triton X-100 in HBSS). The cell suspension was shaken, centrifuged at 15,000 × g at 4 °C for 10 min, and the fluorescence intensity of resultant supernatant was measured in a fluorescence spectrophotometer (F-7000; Hitachi High-Technologies, Tokyo, Japan). The fluorescence intensity was normalized for the protein content of cells. The protein concentration was determined with a Protein Quantification Kit-Wide Range (Dojindo Laboratories, Kumamoto, Japan).

Confocal Microscopy. To observe the colocalization of endosomes and lysosomes, the cells were washed with HBSS and labeled with AlexaFluor-546-conjugated transferrin (Life Technologies) and LysoTracker Red DND-99 (Life Technologies), respectively. To label the endoplasmic reticulum (ER), Golgi apparatus, and mitochondria, the cells were labeled with ER-Tracker Red (Life Technologies), BODIPY TR C_5-ceramide complexed to BSA (Life Technologies), and Mito-Tracker Red FM (Life Technologies), respectively. HeLa cells (5.0×10^4) were plated in 35-mm glass-bottom dishes coated with poly-L-lysine (Matsunami glass, Osaka, Japan) in DMEM containing 10% FBS and 100 U/mL penicillin/streptomycin. After incubation for 48 h (37 °C, 5% CO_2), liposomes were added to the culture medium. At the indicated times after adding liposomes containing fluorescence-labeled DSPC and PEG_{2000}-DSPE, the cells were washed and placed in PBS for confocal microscopy (LSM 780; Carl Zeiss, Oberkochen, Germany). Images were obtained using dedicated software supplied by the manufacturer and exported as tagged image files.

Evaluation of Endocytosis Inhibition. Endocytosis was inhibited by chlorpromazine (50 μM) to inhibit clathrin-mediated endocytosis, genistein (200 μM) and methyl-β-cyclodextrin (MβCD, 2.0 mM) to inhibit caveolae-mediated endocytosis inhibitor, or 5-(*N*-ethyl-*N*-isopropyl) amiloride (50 μM) to inhibit macropinocytosis.[21,22] Each inhibitor was added to the culture medium 30 min before adding the liposomes.

Small Interfering (si)RNA Transfer. Stealth RNAi oligonucleotides (25 mer) were obtained from Life Technologies. The siRNA sequences used in this study are listed in

dx.doi.org/10.1021/mp400505a | *Mol. Pharmaceutics* 2014, 11, 560−567

Table 1 in SI. The Stealth RNAi High GC Negative Control Duplex (Life Technologies) was used as a negative control. The Stealth RNAi oligonucleotides were transfected into cells using Lipofectamine RNAiMAX (Life Technologies). Cells were incubated with each siRNA for 6 h, after which the culture medium was replaced, and the cells were incubated for a further 42 h before adding the liposomes.

Western Blotting. HeLa cells were washed with PBS and lysed in lysis buffer (20 mM Tris-HCl (pH 7.5), 1 mM EDTA, 10% glycerol, and 1% Triton X-100) containing protease inhibitors (2 mM phenylmethylsulfonyl-fluoride and protease inhibitor cocktail; Sigma-Aldrich). The cell lysates were freeze/thawed and centrifuged at 15000*g* at 4 °C for 10 min. Then, we determined the protein concentration of each supernatant using a Protein Quantification Kit-Wide Range (Dojindo Laboratories). For Western blotting, protein samples (20 μg) were heated to 95 °C for 5 min, diluted with loading buffer, and separated by sodium dodecyl sulfate-polyacrylamide gel electrophoresis using 5–20% polyacrylamide gels (SuperSep Ace; Wako Pure Chemical Industries). The separated proteins were transferred to a polyvinylidene fluoride membrane (Immobilon-P; Millipore, Billerica, MA, U.S.A.) by semidry blotting with a Transblot SD (Bio-Rad, Hercules, CA, U.S.A.). To avoid nonspecific binding, the membrane was incubated with Tris-buffered saline containing 5% enhanced chemiluminescence (ECL) Blocking Agent (GE Healthcare). To detect each protein, the primary and secondary antibodies were diluted in Tris-buffered saline containing 5% ECL Blocking Agent. The protein band was detected using ECL reagents (GE Healthcare).

Evaluation of Cytotoxicity. Cytotoxicity was assessed using a WST-8 assay. HeLa cells were plated in a 96-well plate (5.0×10^3 cells/well) in a medium containing 10% FBS and 100 U/mL penicillin/streptomycin. After preincubation for 48 h (37 °C, 5%CO_2), 50 μg/mL of liposomes was added to the culture medium, and the cells were incubated for the specified times. After incubation, cell counting kit-8 solution (Dojindo Laboratories) was added to each well and incubated for 4 h. Absorbance at 450 nm (test wavelength) and 655 nm (reference wavelength) was measured, and the results are expressed as the relative viability (%).

Confirmation of Complex Formation. HeLa cell lysates were prepared according to the Western Blotting section mentioned above. Then, we determined the protein concentration of each supernatant using a Protein Quantification Kit-Wide Range (Dojindo Laboratories). DSPC liposomes were also prepared using DSPC and NBD-labeled DSPC at a molar ratio of 95:5 in 250 mM ammonium sulfate (pH 5.4) according to the Preparation of Liposomes section. The external phase of liposomes was replaced with PBS (pH 8.0) by gel filtration using a Sephadex G-25 column.

Then, 10 μg of HeLa cell lysates were incubated with 1 μg of DOPC liposomes and 0.1 μg of DXR for 24 h at 37 °C to confirm the complex formation with specific protein, phospholipids, and DXR. The resultant mixture was separated and transferred to a polyvinylidene fluoride membrane according to the Western Blotting section. After the blocking and antibody incubation procedure, the protein band was detected using ECL reagents. The band of detected protein, fluorescence-labeled phospholipids, and DXR was visualized using a LAS-4000 mini-imaging system (FUJIFILM Co., Tokyo, Japan).

Statistical Analyses. Results are presented as the mean ± standard deviation (SD) of at least six experiments. Analysis of variance was used to test for statistically significant differences among groups. Comparisons between two groups were done by the Student's *t*-test, and multiple comparisons between the control and test groups were done using Dunnett's test.

RESULTS

Physicochemical Properties. The physicochemical properties of liposomes containing NBD-labeled DSPC or CF-labeled PEG_{2000}-DSPE were determined by measuring the particle sizes, PDI, and ζ-potentials. The mean particle sizes, PDI, and ζ-potentials were approximately 96 nm, 0.08, and 0 mV, respectively (Table 2 in SI).

Intracellular Transport of PEG-Modified Phospholipids. To investigate the intracellular transport mechanisms of PEG_{2000}-DSPE constructing liposomes, the intracellular amounts of CF-labeled PEG_{2000}-DSPE were quantified in HeLa cells. Liposomes were labeled with NBD-labeled DSPC or CF-labeled PEG_{2000}-DSPE, and intracellular uptake into cells was studied by confocal microscopy. DSPC and PEG_{2000}-DSPE were colocalized with endosomes/lysosomes within 1 h of adding each liposome to HeLa cells (Figure 2A in SI). Inhibition of clathrin-mediated endocytosis with chlorpromazine significantly decreased the intracellular concentrations of both lipid components at 2 h after adding the liposomes (Figure 2B in SI).

Intracellular Trafficking Mechanism of PEG-Modified Phospholipids. The intracellular localization of PEG_{2000}-DSPE was compared with that of DSPC by confocal microscopy. As shown in Figure 1, DSPC was colocalized with the ER and Golgi apparatus at 24 h after adding the liposomes to HeLa cells, but was not colocalized with mitochondria (Figure 1, upper panels). By contrast, PEG_{2000}-DSPE was colocalized with the ER, but not with the Golgi apparatus or mitochondria (Figure 1, lower panels).

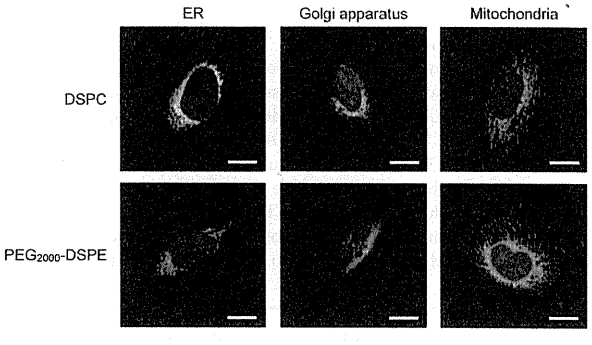

Figure 1. Confocal images showing the intracellular localization of DSPC and PEG_{2000}-DSPE at 24 h after adding liposomes to HeLa cells. Liposomes were labeled with NBD-labeled DSPC (green) or CF-labeled PEG_{2000}-DSPE (green), while the ER, Golgi apparatus, and mitochondria were labeled with ER-Tracker Red (red), BODIPY TR C_5-ceramide (red), and Mito-Tracker Red (red), respectively. Nuclei were counterstained with Hoechst 33342 (blue). Scale bars, 20 μm.

The intracellular trafficking mechanisms of PEG_{2000}-DSPE were compared with that of DSPC. First, we examined the mechanisms controlling trafficking of both phospholipids from the endosome/lysosome to the cytoplasm. In this experiment, suppression of specific proteins using siRNA increased the

intracellular concentrations of phospholipids. In particular, when we suppressed the expression of lipidic trafficking-related proteins, including metastatic lymph-node gene 64 (MLN64) protein, Niemann-Pick C (NPC)1, NPC2, and oxysterol-binding protein-related protein (ORP) 1 (Figure 3 in SI),[23−26] we found that the intracellular concentrations of both phospholipids at 24 h after the addition of liposomes were increased by the suppression of ORP1 (Figure 2A).

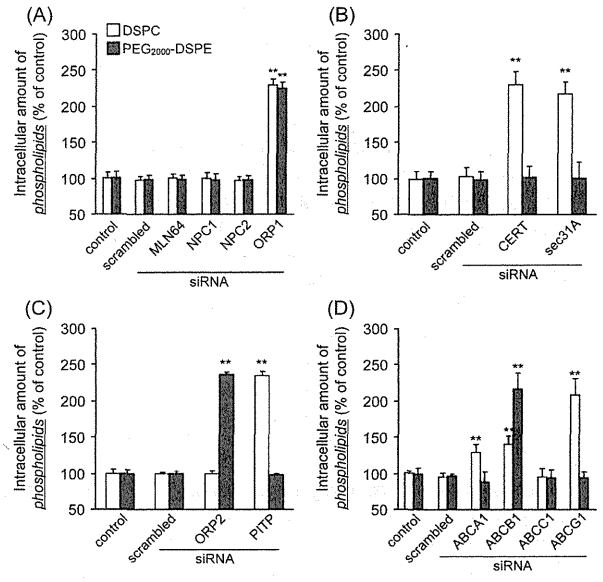

Figure 2. Intracellular trafficking mechanism of DSPC and PEG_{2000}-DSPE in HeLa cells. The intracellular concentrations of DSPC and PEG_{2000}-DSPE were measured 24 h after adding the liposomes to HeLa cells following the suppression of trafficking proteins. siRNAs were used to suppress the expression of proteins involved in the intracellular trafficking from the endosome/lysosome to the cytoplasm (MLN64, NPC1, NPC2, and ORP1) (A), ER−Golgi transport (CERT and sec31A) (B), intracellular trafficking from the ER/Golgi apparatus to the cell membrane (ORP2 and PITP) (C), and extracellular efflux (ABCA1, ABCB1, ABCC1, and ABCG1) (D). siRNAs were transfected using Lipofectamine RNAiMAX. $^{**}P < 0.01$ vs the corresponding control group. Values are presented as mean ± SD ($n = 6$).

Next, we examined the involvement of ER−Golgi transport in the intracellular trafficking of PEG_{2000}-DSPE and DSPC. Suppression of ceramide-transfer protein (CERT) and sec31A, two ER−Golgi transport-related proteins (Figure 3 in SI),[27,28] increased the intracellular concentrations of DSPC at 24 h after adding the liposomes but did not affect the intracellular concentrations of PEG_{2000}-DSPE (Figure 2B).

Then, we investigated the extracellular efflux mechanism of DSPC and PEG_{2000}-DSPE in HeLa cells. To determine the trafficking mechanism from the ER/Golgi apparatus to the cell membrane, we suppressed the expression of ORP2 and phosphatidylinositol transfer protein (PITP), which are involved in the intracellular transport of lipidic molecules (Figure 3 in SI).[29,30] Suppression of ORP2 increased the intracellular concentration of PEG_{2000}-DSPE, but not DSPC, at 24 h after the addition of liposomes (Figure 2C). In experiments in which we suppressed the expression of the ABC transporters (ABCA1, ABCB1, ABCC1, and ABCG1),[31] we found that suppression of ABCB1, but not the other transporters, increased the intracellular concentrations of PEG_{2000}-DSPE at 24 h after the addition of liposomes (Figure 2D). By contrast, only the suppression of ABCG1 increased the intracellular concentrations of DSPC (Figure 2D).

Effects of Liposomal DXR on the Intracellular Trafficking of Phospholipids. We next determined the effects of encapsulating drugs into liposomes on the intracellular trafficking of phospholipids. In this study, we used DXR as the encapsulated drug because it is already clinically used as an anticancer agent in free or liposomal forms.[32] First, we evaluated the effects of DXR on the expression of intracellular trafficking-related proteins in HeLa cells. As shown in Figure 3A, exposure to 0.1 μM DXR for 24 h increased the intracellular expression levels of PITP, ABCA1, and ABCB1 (0.1 μM).

We then investigated the effects of DXR on intracellular trafficking of liposomes generated using phospholipids. In this experiment, we focused on the intracellular proteins whose expression was increased by DXR (i.e., PITP, ABCA1, and ABCB1). As the clinical formulation of liposomal DXR is generated by encapsulating DXR into PEG-modified liposomes,[32] we used PEG-modified liposomes as the model liposomes, and we measured the intracellular concentrations of DSPC, the major component of liposomes. The molar ratio of DSPC, chol, and PEG_{2000}-DSPE was 45:50:5, and the DXR loading efficiency and mean particle size were approximately 96% and 100 nm, respectively. Figure 3B shows that suppression of PITP expression, a protein involved in intracellular transport from the ER/Golgi apparatus to the cell membrane (Figure 3 in SI), resulted in greater intracellular concentrations of phospholipids derived from DXR-loaded liposomes as compared with phospholipids derived from unloaded liposomes. Regarding extracellular efflux, the intracellular concentrations of phospholipids derived from DXR-loaded liposomes were higher than that of phospholipids from unloaded liposomes when we suppressed the expression of ABCA1 and ABCB1 (Figure 3C).

Effects of Lipid Components on Intracellular Trafficking and the Cytotoxicity of DXR. We finally examined the effects of liposomes generated using phospholipids on the intracellular transport of DXR. In these experiments, we used PEG-modified liposomes as the model liposomes. Suppression of proteins involved in endosome/lysosome cytoplasm transport or ER−Golgi transport did not affect the intracellular concentrations of DXR transported by PEG-modified liposomes (data not shown). As shown in A and B of Figure 4, the intracellular concentrations of DXR transported by PEG-modified liposomes was increased when the expression of PITP and ABCB1 was suppressed. Moreover, the cytotoxicity of DXR transported by PEG-modified liposomes was increased by suppressing PITP and ABCB1 expression in HeLa cells (Figure 4C). Similar results were obtained in the experiments using DXR transported by unmodified liposomes (data not shown).

The increase in intracellular concentration of DXR after suppressing ABCB1 expression is attributed to the previous reports that DXR is the substrate of ABCB1.[33−35] By contrast, although PITP is involved in the intracellular transport of phospholipids (Figure 2C), PITP was not involved in the intracellular trafficking of DXR (Figure 4 in SI).

Next, we investigated the formation of complexes of PITP, phospholipids, and DXR. After incubation in various conditions aimed at promoting complex formation, we found that DSPC formed a complex with PITP, but DXR did not form a complex

dx.doi.org/10.1021/mp400505a | Mol. Pharmaceutics 2014, 11, 560−567

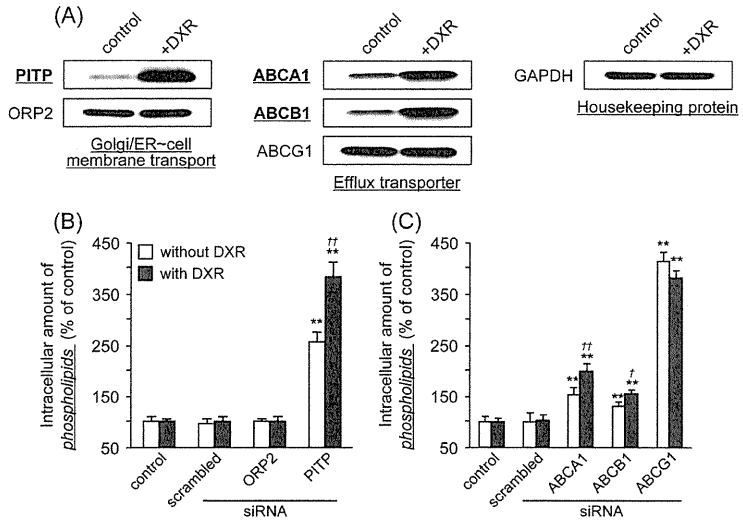

Figure 3. Effects of DXR-encapsulated liposomes on the intracellular trafficking of phospholipids in HeLa. (A) Effects of DXR on the expression of proteins involved in intracellular trafficking of phospholipids. Cells were incubated for 24 h in the presence of a low concentration of DXR (0.05 μg/mL) and protein expression was determined by Western blotting. (B, C) Intracellular concentrations of phospholipids at 24 h after adding liposomes to HeLa cells with suppression of trafficking-related proteins. Liposomes were labeled with ATTO-647N DOPE. siRNAs were used to suppress the expression of proteins involved in intracellular trafficking from the ER/Golgi apparatus to the cell membrane (ORP2 and PITP) (B), or extracellular efflux (ABCA1, ABCB1, and ABCG1) (C). siRNAs were transfected using Lipofectamine RNAiMAX. $^{**}P < 0.01$ vs the corresponding control group; $^{\dagger}P < 0.05$; $^{\dagger\dagger}P < 0.01$ vs the DXR-untreated group. Values are presented as mean ± SD ($n = 6$).

with PITP (Figure 4D). However, DXR did form a complex with PITP in the presence of DSPC (Figure 4D). Moreover, as shown in Figure 4E, the intracellular concentrations of DXR increased when PITP expression was suppressed following coincubation with DSPC liposomes. These observations suggest that DXR transported by liposomes forms complexes with PITP and phospholipids, and this complex is involved in the intracellular trafficking of transported DXR.

DISCUSSION

In this study, we first investigated the intracellular trafficking of PEG-modified phospholipids used to generate liposomes. We have previously reported on the intracellular trafficking mechanism of phospholipids and chols, the major components of liposomes.[18] In this study, we evaluated the effects of PEG modification on the intracellular trafficking of phospholipids. As shown in Figure 1, following intracellular uptake of PEG-modified DSPE *via* endocytosis, although DSPC was localized to the ER and Golgi apparatus, PEG-modified DSPE was only localized to the ER. Moreover, the intracellular concentrations of PEG_{2000}-DSPE were not affected by suppressing CERT and sec31A expression (Figures 2B), suggesting that ER–Golgi transport is not involved in the intracellular trafficking of PEG-modified phospholipids. Although DSPC was transported to the cell membrane by PITP and extracellular effluxed *via* ABCG1, PEG-modified DSPE was transported to the cell membrane by ORP2 and extracellular effluxed *via* ABCB1 (Figures 2C and 2D). Thus, we showed that PEG modification had remarkable effects on the intracellular trafficking of phospholipids.

Next, we evaluated the effects of encapsulating drugs into liposomes on the intracellular trafficking of liposomal phospholipids. In this series of experiments, we used DXR as the encapsulated drug because it is widely used as an anticancer agent, and liposomal formulations are in clinical use.[32] We found that exposure to a low concentration of DXR for 24 h increased the expression of PITP, ABCA1, and ABCB1 in HeLa cells (Figure 3A). Furthermore, the intracellular concentrations of liposomal phospholipids derived from DXR-loaded liposomes were increased by the suppression of PITP expression (Figure 3B). These results suggest that DXR enhances the extracellular efflux of liposomal phospholipids by enhancing PITP expression. We also found that the intracellular concentrations of liposomal phospholipids were increased by DXR following suppression of ABCA1 and ABCB1 expression (Figure 3C). These findings suggest that DXR enhances the activities of ABCA1 and ABCB1 in terms of extracellular efflux of phospholipids. It was previously reported that low concentrations of DXR induce the expression of various ABC transporters.[14−17] Therefore, our results suggest that DXR encapsulated into liposomes enhances ABCA1 and ABCB1 expression, which consequently increases the extracellular efflux of phospholipids. Various anticancer agents were reported to enhance the expression of ABC transporters, including P-gp.[14−17] In a previous study[18] and the present study, we showed that the major liposomal components underwent extracellular efflux *via* ABC transporters, and competitively inhibited ABC transporter-mediated extracellular efflux of encapsulated drugs.[18] Considering these findings, we think that, although DXR increases the expression of P-gp, the extracellular efflux of DXR *via* P-gp will be suppressed by competitive inhibition of P-gp by phospholipids. These events might ultimately enhance the anticancer effects of DXR .

We also investigated the effects of liposomal phospholipids on the intracellular trafficking and cytotoxicity of DXR. In experiments aimed at determining the effects of various proteins on DXR trafficking, we found that the intracellular concentrations of DXR were only increased when we suppressed ABCB1 expression (Figure 4 in SI). These results are consistent with those of earlier reports showing that DXR is